Published for SISSA by Springer

Received: *April 5, 2024*
Revised: *August 1, 2024*
Accepted: *September 27, 2024*
Published: *October 16, 2024*

Quiver tails and brane webs

Sebastián Franco[a,b,c] **and Diego Rodríguez-Gómez**[d,e]

[a]*Physics Department, The City College of the CUNY, 160 Convent Avenue, New York, NY 10031, U.S.A.*
[b]*Physics Program, The Graduate School and University Center, The City University of New York, 365 Fifth Avenue, New York NY 10016, U.S.A.*
[c]*Initiative for the Theoretical Sciences, The Graduate School and University Center, The City University of New York, 365 Fifth Avenue, New York NY 10016, U.S.A.*
[d]*Department of Physics, Universidad de Oviedo, C/ Federico García Lorca 18, 33007 Oviedo, Spain*
[e]*Instituto Universitario de Ciencias y Tecnologías Espaciales de Asturias (ICTEA), C/ de la Independencia 13, 33004 Oviedo, Spain*

E-mail: sfranco@ccny.cuny.edu, d.rodriguez.gomez@uniovi.es

Abstract: A new type of quiver theories, denoted twin quivers, was recently introduced for studying 5*d* SCFTs engineered by webs of 5-branes ending on 7-branes. Twin quivers provide an alternative perspective on various aspects of such webs, including Hanany-Witten moves and the *s*-rule. More ambitiously, they can be regarded as a first step towards the construction of combinatorial objects, generalizing brane tilings, encoding the corresponding BPS quivers. This paper continues the investigation of twin quivers, focusing on their non-uniqueness, which stems from the multiplicity of toric phases for a given toric Calabi-Yau 3-fold. We find that the different twin quivers are necessary for describing what we call quiver tails, which in turn correspond to certain sub-configurations in the webs. More generally, the multiplicity of twin quivers captures the roots of the Higgs branch in the extended Coulomb branch of 5*d* theories.

Keywords: Brane Dynamics in Gauge Theories, Field Theories in Higher Dimensions, Supersymmetric Gauge Theory, Supersymmetry and Duality

ArXiv ePrint: 2310.10724

Open Access, © The Authors.
Article funded by SCOAP[3].

https://doi.org/10.1007/JHEP10(2024)118

JHEP10(2024)118

Contents

1 Introduction

Quantum Field Theories in 5*d* are notoriously hard to construct. In the case of supersymmetric theories, String/M Theory provides various approaches to engineer 5*d* Superconformal Field Theories (SCFTs). For instance, M-theory on a toric Calabi-Yau 3-fold (CY_3) engineers a 5*d* SCFT in the transverse directions [1, 2].[1] An alternative realization of 5*d* SCFTs is on the worldvolume of systems of webs of (p, q) 5-branes in type IIB String Theory [18, 19]. In fact, it turns out that these two approaches are related by dualities, and the (p, q)-web corresponds to the spine of the toric diagram for the CY_3 [19, 20].

An interesting piece of information about a 5*d* SCFT is its spectrum of BPS particles, which can be encoded in a *BPS quiver*.[2] It turns out that the BPS quiver for a 5*d* theory

[1] The geometric engineering of 5*d* theories has been thoroughly studied beyond the toric case. See for instance [3–17].

[2] See [21] for an introduction to BPS quivers.

JHEP10(2024)118

engineered via M-theory on a toric CY_3 coincides with the quiver on the worldvolume of D3-branes probing the same geometry [22].[3] The latter is a problem with a long and honored history that culminated with the introduction of *brane tilings* (also known as dimer models), which significantly simplify the connection between geometry and quiver theories [23, 24]. Brane tilings can be represented by bipartite graphs on a 2-torus that encode the quiver and superpotential of the corresponding gauge theories and, simultaneously, reduce the determination of the associated CY_3 to a combinatorial problem. They are physical brane configurations, connected via T-duality to the D3-branes on toric CY_3's.

Brane tilings have been generalized to *bipartite field theories* (BFTs), a class of quiver theories defined by bipartite graphs on Riemann surfaces, which enjoy many of the combinatorial properties and connections to toric geometry of brane tilings [25–29].[4] In the context of BFTs, there is an interesting operation known as *untwisting*, which maps a bipartite graph on Riemann surface to a new embedding of the same graph on a generically different Riemann surface. For the brane tiling encoding the BPS quiver for a $5d$ SCFT engineered by M-theory on a toric CY_3, the BFT obtained by untwisting is closely related to the (p, q)-web that engineers it. This connection is related to mirror symmetry and is another manifestation of the duality connecting both String/M Theory realizations of the $5d$ SCFT.

To visualize the Higgs branch of $5d$ theories, it is useful to terminate the legs of (p, q)-webs on suitable 7-branes. This opens up the possibility of having more than one 5-brane terminating on a given 7-brane. This imposes an extra constraint due to the s-rule, which has far reaching consequences. In these cases, the (p, q)-web can be regarded as the spine of a generalization of a toric diagram in which boundary edges are merged. The resulting polytopes, which include white and black dots, are called *generalized toric polygons* (GTPs) [31–33]. GTPs raise natural new questions, including their geometric interpretation and whether the corresponding BPS quivers are captured by some objects generalizing brane tilings.

Interesting progress along these lines was made recently in [34] and [35]. *Twin quivers*, a new type of quiver theories that provide an alternative perspective on various aspects of the webs of 5- and 7-branes associated to generic GTPs, including their mutations and the s-rule, were introduced in [35]. Various methods for the construction of twin quivers were introduced in [35]. Untwisting of brane tilings plays an important role in them. In view of the toric case, it is natural to expect that twin quivers provide a first step towards the BPS quivers of $5d$ SCFTs associated to GTPs and their geometric description.

This paper continues the investigation of twin quivers, focusing on the physical significance of the ones obtained from brane tilings associated to multiple toric phases of a single underlying CY_3. This multiplicity was already noticed in [35]. Remarkably, we find that the different twin quivers correspond to different chambers in the extended Coulomb branch of the $5d$ SCFT sensitive to the roots of the Higgs branch. As a consequence, this provides a method for constructing GTPs including white dots starting from standard toric theories.

This paper is organized as follows. Section 2 reviews the brane web and geometric realizations of $5d$ theories, GTPs and twin quivers. Section 3 provides a first approach to the issue of twin quivers arising from multiple toric phases. Section 4 starts the study

[3] To be precise, the BPS quiver is for the $5d$ theory on $S^1 \times \mathbb{R}^{1,3}$.

[4] A closely related class of theories was considered in [30].

JHEP10(2024)118

of brane webs, twin quivers and their mutations for theories associated to non-chiral $\mathbb{Z}_N$ orbifolds of the conifold. Section 5 considers additional toric phases for the same orbifolds of the conifolds, introducing the concept of quiver tails. It also discusses how to assign twin quivers for different points on the extended Coulomb branch using mirror symmetry. In addition it considers the decoupling of tails and connects it to the operation of node merging in the construction of twin quivers. Section 6 presents several additional examples. Section 7 discusses the general structure of quiver tails obtained by mutation of twin quivers containing an arbitrary number of bidirectional arrows between nodes. Section 8 proposes the combination of quiver tails and gluing for generating twin quivers for general GTPs. Finally, section 9 presents our conclusions and future directions.

2 Brane webs and twin quivers for 5*d* theories

5d SCFTs can be engineered on webs of 5-branes in Type IIB String Theory. Part of the information on these webs can be efficiently encoded in the so-called *generalized toric polygons* (GTPs) [31–33]. In turn, every GTP can be associated to a *twin quiver*, which provide, for example, an alternative perspective on the mutations and s-rule of the associated webs. In this section we review the engineering of 5d SCFTs using brane webs, and the construction of the associated GTPs and twin quivers.

2.1 Basics on 5-brane webs for 5*d* SCFTs

Webs of 5-branes in Type IIB String Theory provide a powerful tool for studying the dynamics of a large class of 5d SCFTs theories [19]. The 5-branes fully extend on the (01234) directions, span a line on the (56) plane and sit at the point $x^7 = x^8 = x^9 = 0$ in the remaining directions. Most of the interesting physics is captured by the configuration on the (56) plane, to which we will refer as the plane of the web. The slopes of 5-branes on this plane are determined by their (p, q) charges, with their intersections subject to (p, q) charge conservation at every vertex. The (p, q) charges of every 5-brane are mutually coprime. The external (p, q) 5-branes of the web, to which we will often refer as legs, are assumed to terminate on a $[p, q]$ 7-brane. Each 7-brane extends on the (01234789) directions and is pointlike on the plane of the web. Multiple (p, q) 5-branes can end on a single $[p, q]$ 7-brane. In those cases, there is an extra constraint coming from supersymmetry in the form of the s-rule.[5] In the context at hand, the s-rule states that a maximum of $|ps - qr|$ (p, q) 5-branes can be supersymmetrically suspended between a $[p, q]$ 7-brane and an (r, s) 5-brane [31].

It is important to bear in mind that 7-branes come with a branch cut for the axio-dilaton on the plane of the web. As it is standard, we will assume that such branch cuts point radially away from the web, without crossing it. In addition, the length of a leg is not a parameter of

[5]The s-rule was originally introduced in [36] for D3-branes linked between D5/NS5, and it was subsequently generalized to various other contexts. In [31], it was formulated for generic (p, q) 5-branes ending on $[r, s]$ 7-branes (in particular, in terms of generalized toric polygons, later developed in [32]). More recently, it was discussed in [37] using the fact that the SUSY condition for 5-branes ending on 7-branes is identical to that of (p, q) strings ending on $[r, s]$ 7-branes [38].

JHEP10(2024)118

the low energy SCFT.[6] Using this fact, we implicitly assume large legs, i.e. very separated 7-branes, so that the axio-dilaton is approximately constant over the scales of the web. This justifies neglecting the curvature associated to the 7-branes.

5d SCFTs are intrinsically strongly coupled and isolated. They generically have a moduli space which corresponds to the possible deformations of the web which do not change the positions of the external 7-branes from which the web is suspended. In turn, the deformations which change the positions of the 7-branes correspond to relevant deformations. Such deformations trigger an RG flow to an IR effective theory, which sometimes corresponds to a standard supersymmetric gauge theory, which in 5d is IR free.

The moduli space is divided into the Coulomb and Higgs branches, which are captured by different deformations of the underlying brane web. On the Coulomb branch, the web is deformed inside its plane. When the 5d SCFT admits a deformation to a gauge theory, these moduli space directions correspond to the standard Coulomb branch, in which scalars in vector multiplets take non-zero VEVs. On the other hand, along the Higgs branch, the web is separated into consistent sub-webs which slide along the 7-branes in the (789) directions. When the 5d SCFT admits a deformation to a gauge theory, these directions correspond to the standard Higgs branch, where scalars in hypermultiplets take VEVs.

When the 5d SCFT has a deformation to a gauge theory, relevant deformations can be regarded as supersymmetric VEVs for scalars in background vector multiplets coupled to the global symmetries of the gauge theory. For this reason, the combination of the Coulomb branch and relevant deformations is often referred to as the extended Coulomb branch.

Importantly for our purposes, the Higgs branch typically only touches the (extended) Coulomb branch along some lower-dimensional manifold termed the *root of the Higgs branch*. A prototypical example is the rank 1 E_1 theory in section 6.2, where the (extended) Coulomb branch touches the Higgs branch only at the origin, and consequently the Higgs branch can only be entered at the origin of the (extended) Coulomb branch.

2.1.1 Webs and Hanany-Witten moves

The 5-brane web engineering a given 5d SCFT is not unique. To begin with, the $\mathrm{SL}(2,\mathbb{Z})$ duality of Type IIB String Theory connects webs whose legs have charges differing by a global $\mathrm{SL}(2,\mathbb{Z})$ transformation. Let us cyclically order the legs counterclockwise, with an arbitrary leg chosen as first. Consider two webs with legs whose charges are $\ell_i = (p_i, q_i)$ and $\ell'_i = (p'_i, q'_i)$, with $i = 1, \ldots, L$, respectively. The two webs define the same 5d SCFT if there is a matrix $U \in \mathrm{SL}(2,\mathbb{Z})$ such that $\ell'_i = U\ell_i$ for all i.

More interestingly, webs can be related by crossing 7-branes. As mentioned above, since the length of a leg is not a parameter in the low energy SCFT, one may shrink it by moving

[6] This is completely analogous to the position of flavor D6-branes in the direction parallel to color D3-branes in the brane engineering of 3d gauge theories introduced in the seminal paper by Hanany and Witten [36] (we would like to thank Amihay Hanany for discussion of this point). Not only this position does not have a physical meaning in the gauge theory, but the study of what happens as it is varied lead to the discovery of the Hanany-Witten transition. Similarly, 7-branes in our setups can be freely moved along their prongs, in particular crossing them to the other side of the web, without changing the low energy 5d theory. It is precisely this freedom that leads to the (in principle) infinitely many different descriptions of the same theory connected by 7-brane motions that we discuss in this work.

JHEP10(2024)118

the corresponding 7-brane along it until eventually crossing the rest of the web and sending it away to a very large distance in the opposite direction. In order to comply with the standard presentation discussed above, one has to rotate the branch cut of the crossed 7-brane, which, as it sweeps other 7-branes, changes them accordingly (and consequently the 5-branes). More precisely, the monodromy of a $[p_j, q_j]$ 7-brane is

$$M_{(p_j,q_j)} = \begin{pmatrix} 1 - p_j q_j & p_j^2 \\ -q_j^2 & 1 + p_j q_j \end{pmatrix} . \tag{2.1}$$

Then, when the monodromy sweeps a $[p_i, q_i]$ 7-brane counter-clockwise, it gets transformed into a $[p_i', q_i']^T = M_{(p_j,q_j)} [p_i, q_i]^T$ 7-brane (if it is swept clockwise the transformation matrix is $M^{-1}_{p_j,q_j}$).[7] Of course, the (p_i, q_i) 5-branes ending on it change accordingly. Note that in the process the crossed 7-brane may require a different number of 5-branes ending on it than originally, which is due to the Hanany-Witten effect [36].

Equivalently, the transition described above can be phrased as follows. First of all, let us define the intersection number between two 7-branes j and i as follows

$$\langle \ell_j, \ell_i \rangle = \det \begin{pmatrix} p_j & q_j \\ p_i & q_i \end{pmatrix} . \tag{2.2}$$

The charge vectors satisfy the following relation

$$\sum_s N_i \ell_i = 0 \,, \tag{2.3}$$

where N_i is the number of 5-branes terminating on 7-brane i. Equation (2.3) is simply the equilibrium condition for the (p, q)-web.

Crossing brane j corresponds to changing the charge vectors as follows

$$\begin{aligned} & \ell_j' = -\ell_j \\ i \neq j : \quad & \ell_i' = \ell_i + \langle \ell_j, \ell_i \rangle \ell_j \qquad \text{for } \langle \ell_j, \ell_i \rangle > 0 \\ & \ell_i' = \ell_i \qquad\qquad\qquad\quad \text{otherwise} \end{aligned} \tag{2.4}$$

In order to satisfy (2.3) after the mutation, N_j must transform according to

$$N_j' = \sum_{i \in L_+} N_i \langle \ell_j, \ell_i \rangle - N_j \,, \tag{2.5}$$

where L_+ is the set of 7-branes with $\langle \ell_j, \ell_i \rangle > 0$. It is straightforward to show that (2.4) is equivalent to (2.1). There is an equivalent transformation in which, for a given crossed 7-brane j, the roles of the ℓ_i's with $\langle \ell_j, \ell_i \rangle > 0$ and $\langle \ell_j, \ell_i \rangle < 0$ are exchanged in (2.4). More precisely, this corresponds to replacing $\langle \ell_j, \ell_i \rangle$ by $-\langle \ell_j, \ell_i \rangle$ everywhere in (2.4) and to moving the branch cut around the web in the opposite direction, i.e. using the inverse of the monodromy matrix.

[7] Here we imagine a $[p_j, q_j]$ 7-brane to be moved along its prong until crossed, and then its monodromy rotated, thus sweeping the $[p_i, q_i]$ 7-brane.

JHEP10(2024)118

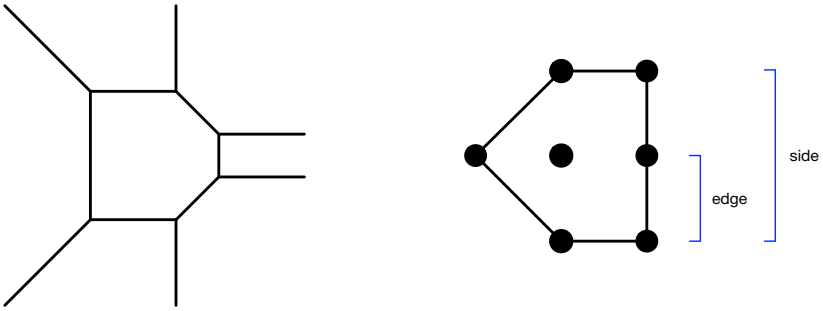

Figure 1. A brane web and the corresponding toric diagram. The figure illustrates the concepts of edge and side of the toric diagram.

2.2 Geometric engineering and GTPs

Focusing on webs in which every 5-brane terminates on a different 7-brane, we can neglect the 7-branes and regard the external legs as semi-infinite segments. Such (p, q)-webs are related, via graph dualization, to toric diagrams of toric CY 3-folds.[8] Indeed, the same $5d$ theory can alternatively be obtained as the low energy limit of M-theory on $\mathbb{R}^{1,4}$ times the local CY 3-fold associated to the toric diagram [19, 20]. From this perspective, the extended Coulomb branch corresponds to the Kähler cone of the CY 3-fold (see e.g. [39] for a detailed account). The interesting relations do not stop there, since the BPS spectrum of the $5d$ theory is encoded in a quiver theory that is precisely the one defined by the brane tiling corresponding to the toric diagram, i.e. the one for the $4d$ $\mathcal{N} = 1$ gauge theory on the worldvolume of D3-branes probing the CY_3 [22]. Figure 1 shows a (p, q)-web and the related toric diagram.

While discussing the boundaries of toric diagrams, it is convenient to introduce the concepts of *sides* and *edges*. We refer to a side as the line connecting two consecutive corners of the toric diagram. Within a given side, an edge is a segment between two consecutive points in the toric diagram. The difference between the two types of objects becomes relevant for sides consisting of more than one edge. Edges of the toric diagram are in one-to-one correspondence with legs of the dual (p, q)-web. Whenever a side of a toric diagram contains multiple edges, the (p, q)-web has the same number of parallel legs. Figure 1 illustrates these ideas in an example.

In order to accommodate for multiplicities larger than 1, *generalized toric polygons* (GTPs) where proposed in [31] as generalizations of toric diagrams that encode such brane configurations. 7-branes are represented on the boundary of a GTP as follows. If two parallel legs of the (p, q)-web terminate on the same 7-brane, the dot that separates the corresponding edges in the GTP is colored white. Similarly, n consecutive edges on a given side of the GTP separated by $n - 1$ white dots represent n parallel legs of the web terminating on a single 7-brane.[9] Figure 2 shows a simple example.

[8] More precisely, graph dualization connects a triangulation of the toric diagram to a (p, q)-web. Different triangulations map to different resolutions of the CY_3 and to different points on the extended Coulomb branch of the $5d$ theory.

[9] Similarly, white dots in the interior of a GTP capture the details of the 5-branes in the interior of the web, including the possible Coulomb branch directions. We refer the reader to [31] as well as [32, 33] for details.

JHEP10(2024)118

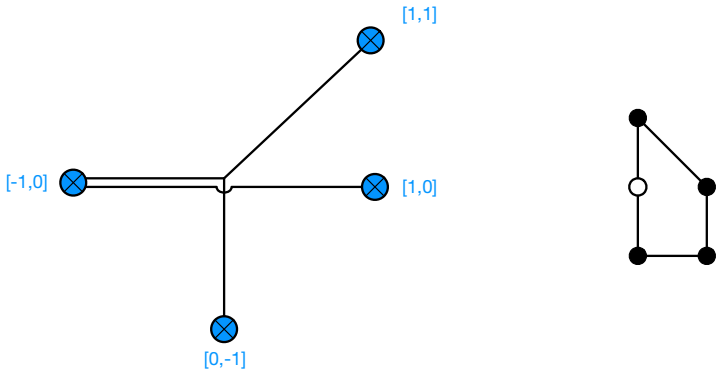

Figure 2. A brane web in which multiple 5-branes terminate on the same 7-brane and the corresponding GTP.

2.3 Constructing twin quivers

Twin quivers were introduced in [35] and provide a powerful new tool for the study of webs of 5- and 7-branes (equivalently GTPs) and the corresponding $5d$ theories.[10] Twin quivers have a node for every 7-brane, whose rank is given by the number of 5-branes ending on it. A salient feature of twin quivers is that Hanany-Witten-type transitions on brane webs translate into quiver mutations, i.e. Seiberg duality.[11] On a related note, they give an alternative perspective on the generalized s-rule that identifies supersymmetric brane configurations. In this section, we quickly review a method for constructing the twin quiver associated to general webs of 5-branes and 7-branes, equivalently to general GTPs, which was introduced in [35]. Twin quivers heavily rely on various objects and operations that are standard in the study of brane tilings (see below for more comments on brane tilings) and, more generally, bipartite field theories BFTs [25–29]. They include zig-zag paths, untwisting and the connection between zig-zag paths and geometry. We refer the reader to [35] for a review of these ideas focused on applications to twin quivers, additional details and alternative algorithms for determining twin quivers.

Let us consider a general brane web and denote as i the set of 5-brane legs with a given orientation (p_i, q_i) and indicate the number of such legs as N_i.[12] The configuration also contains $J_i \leq N_i$ (p_i, q_i) 7-branes (denote each such leg by $\vec{\ell}_A^{(i)} = (p_i, q_i)$, with $A = 1, \ldots, J_i$) on which these 5-branes can end. The multiplicities, i.e. the numbers of 5-branes terminating on each of the 7-branes, are $k_A^{(i)} = \{k_1^{(i)}, \ldots, k_{J_i}^{(i)}\}$. We can alternatively discuss such a web in GTP language, where it maps to a polytope with a general array of black and white dots on

[10] As explained in [35], the applications of twin quivers go well beyond such brane webs and $5d$ theories.

[11] We refer the reader to [40, 41] to detailed discussions of Seiberg duality for quivers, including the transformation of the superpotential. In this paper we will formally apply the mutation rule even on U(1) nodes of the quivers.

[12] In [35], zig-zag paths and the corresponding nodes in twin quivers were indicated with tilded indices, to distinguish them from faces and quiver nodes in the *original* theories. Here, original refers to the theories defined by the brane tilings associated to the toric diagram under consideration, which are connected to the twin theories by untwisting. Since this paper is primarily devoted to twin quivers, we will omit the tildes to simplify the notation. In the few occasions in which we present the original theories, such as figure 27, we expect that the meaning of indices will be clear from the context.

JHEP10(2024)118

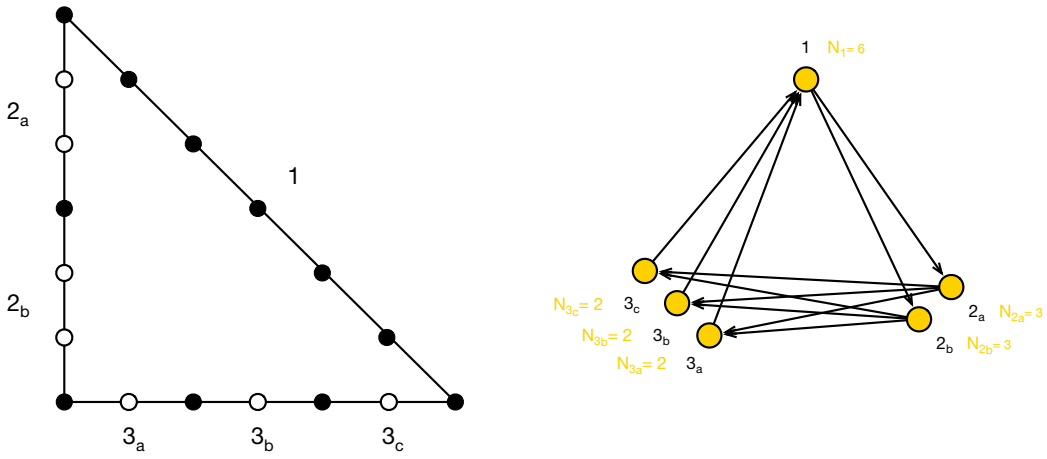

Figure 3. A GTP, for which we only show the boundary, and the corresponding twin quiver.

its boundary. Each side i contain N_i edges, which are partitioned into subsets containing $\{k_1^{(i)}, \ldots, k_{J_i}^{(i)}\}$ edges, such that the edges in each subset are separated by white dots and different subsets are separated by black dots.

The associated twin quiver is constructed as follows:

1. Regarding the polytope under consideration as a toric diagram (namely with all black dots), construct the corresponding brane tiling.

2. Generate the BFT for $\tilde{Q}_{\mathrm{T}}$ by untwisting.[13] This quiver has one node for every zig-zag path of the original tiling/edge of the original toric diagram.

3. Finally, the N_i nodes associated to every side with N_i edges in the original toric diagram are merged into J_i nodes of ranks $k_1^{(i)}, \ldots, k_{J_i}^{(i)}$.

While we have primarily focused on the quiver diagram, the procedure outlined above can be refined to also produce the superpotential of the resulting twin quiver theory.[14] figure 3 presents an example illustrating basic features of this construction.

As anticipated above, the twin quiver constructed in this way has a $\mathrm{U}(k_A^{(i)})$ gauge group for each external leg with charge vector $\vec{\ell}_A^{(i)}$ and $N_{A,B}^{i,j} = \langle \vec{\ell}_A^{(i)}, \vec{\ell}_B^{(j)} \rangle$ bifundamentals from node $\mathrm{U}(k_A^{(i)})$ to node $\mathrm{U}(k_B^{(j)})$ if $N_{A,B}^{i,j} > 0$ and in the opposite direction if $N_{A,B}^{i,j} < 0$.

3 Twin quivers for different toric phases

In the previous section, we reviewed the construction of the twin quiver associated to a GTP/brane web. The construction involves the determination of a brane tiling/quiver theory Q for a standard toric diagram, which is followed by untwisting and certain identifications in the case of GTPs containing white dots. Generically, a given toric diagram is associated to multiple brane tilings. These different quiver theories are known as *toric phases* and are

[13] By this, we mean the corresponding bipartite graph on a Riemann surface.

[14] This algorithm will be reported in future work.

JHEP10(2024)118

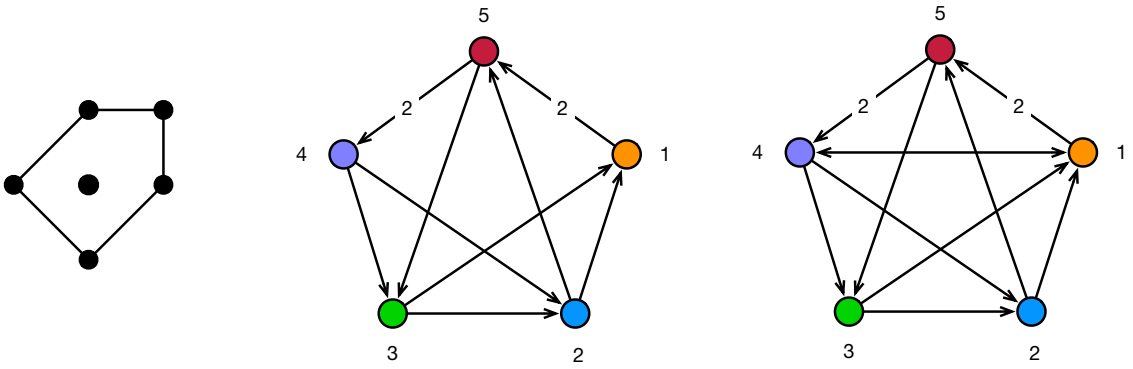

Figure 4. The dP_2 geometry has two toric phases, which gives rise to the two twin quivers shown in this figure upon untwisting.

connected to each other by mutations (or, equivalently, Seiberg duality) on toric nodes..[15] At present, it is not known whether it is possible to determine the number of toric phases exclusively from the geometry. It natural to ask how the non-uniqueness of Q reflects on the twin quivers $\tilde{Q}$. These issue was first noticed and addressed in [35], to where we refer the reader for further details. It should be noted that while the original brane tiling lives on a 2-torus (for all phases), the bipartite graphs that describe the twin theories upon untwisting live on a Riemann surface whose genus is equal to the number of internal points of the toric diagram of the original Calabi-Yau 3-fold [42]. While this surface is not necessarily a 2-torus, it is clearly the same for all the twin theories associated to the different toric phases.

In [35] it was shown that the twin quivers for a given GTP constructed using different toric phases of Q differ by bidirectional arrows.[16] This phenomenon can be understood in general using the construction of twin quivers of section 2. After replacing the GTP by a toric diagram (if necessary), let us refer to the two toric phases associated to it as $Q_{\mathrm{T},(\mathrm{a})}$ and $Q_{\mathrm{T},(\mathrm{b})}$. The (sequence of) Seiberg duality transformation(s) connecting $Q_{\mathrm{T},(\mathrm{a})}$ and $Q_{\mathrm{T}(\mathrm{b})}$ corresponds to a reorganization of some of the zig-zag paths that preserves their homology [43]. In this process, the intersections between zig-zag paths change, but they appear/disappear in pairs, with opposite signs. Since nodes in $\tilde{Q}_{\mathrm{T},(\mathrm{a})}$ and $\tilde{Q}_{\mathrm{T}(\mathrm{b})}$ correspond to zig-zags, they only differ by bidirectional arrows. This property is preserved if the GTP contains white dots and, correspondingly, nodes in the twin quiver are combined into higher rank ones to form $\tilde{Q}_{\mathrm{GTP},(\mathrm{a})}$ and $\tilde{Q}_{\mathrm{GTP}(\mathrm{b})}$. Figure 4 illustrate the non-uniqueness of the twin quivers in an explicit example, in which the GTP is simply the standard toric diagram for dP_2. This example will be revisited in section 6.3.

It is important to emphasize that, as the example in figure 4 illustrates, the non-uniqueness of the twin quivers is a generic phenomenon, which is present even for ordinary toric diagrams/web configurations. In other words, it is unrelated to whether the brane

[15] Following the convention in the literature, we use the term toric node to indicate a node in the quiver with two incoming and two outgoing chiral arrows. Equivalently, it corresponds to a four sided face in the brane tiling. These nodes are special in that a Seiberg duality on them results in another quiver theory described by a brane tiling [23].

[16] It is also possible to understand the superpotentials of these different twin quivers, but we leave a more detailed discussion for future work.

JHEP10(2024)118

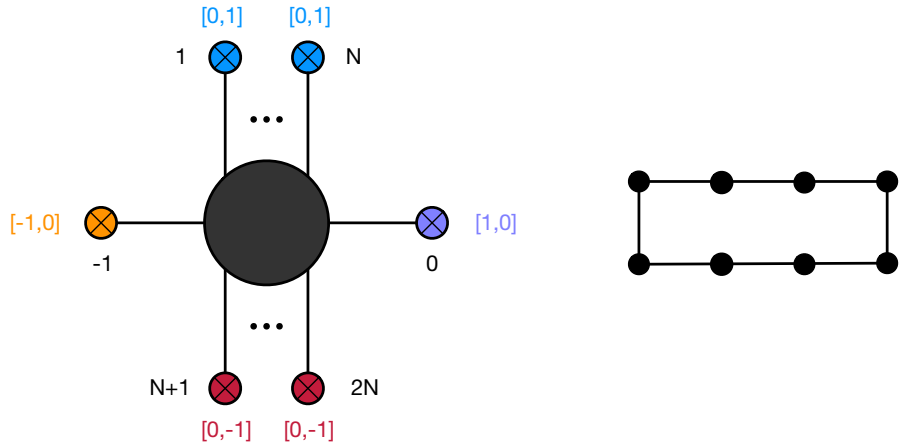

Figure 5. Brane web for N^2 hypermultiplets. On the right, the dual toric diagram is the one for a non-chiral $\mathbb{Z}_N$ orbifold of the conifold (here shown for $N = 3$).

web have multiple legs terminating on the same 7-brane or not. This is also reflected in the fact that the $N^{i,j}_{A,B}$ introduced above are only sensitive to the antisymmetric part of the connection matrix, and thus insensitive to bidirectional arrows in the quiver.

In this paper we will investigate the physical significance of the multiple twin quivers, i.e. what properties or the corresponding brane webs they capture. We will see that these capture different regions of the extended Coulomb branch of the $5d$ theory.

4 Conifold/$\mathbb{Z}_N$

Let us consider the brane web shown in figure 5, which describes N^2 free hypermultiplets in $5d$. This web can also be regarded as the $M = 1$ case of the $+_{N,M}$ family of theories introduced in [44]. The corresponding GTP, is the ordinary toric diagram for a non-chiral $\mathbb{Z}_N$ orbifold of the conifold.

It is straightforward to construct the corresponding brane tiling, which is shown in figure 6.[17] It is obtained by appending N copies of the unit cell describing the conifold theory.[18] The orbifold action under consideration translates into the details of how these copies are combined (see e.g. [23, 45, 47]).

The twin theory is obtained by untwisting the brane tiling. As expected from the corresponding web and toric diagrams, it corresponds to a bipartite graph on a sphere with $2N + 2$ punctures, each of which can be identified with a leg of the web. Figure 7 shows the untwisted graph for $N = 3$.

The twin quiver, shown in figure 8, has a node for every 7-brane in the configuration. In order simplify figures, throughout the paper the rank of quiver nodes will be 1 unless

[17]The winding numbers of the zig-zag paths correspond to the (p, q) charges of the corresponding legs in the web. Other equivalent choices of the unit cell result in (p, q) charges that differ from the ones in figure 5 by an $\mathrm{SL}(2, \mathbb{Z})$ transformation.

[18]The brane tiling for the conifold is a square lattice [23]. In this case, we have used the fact that the brane tilings for the orbifolds of any toric CY_3 are obtained by appropriately combining copies of the brane tiling of the original CY_3 [23, 45] (see also [46–48] for additional explicit examples).

JHEP10(2024)118

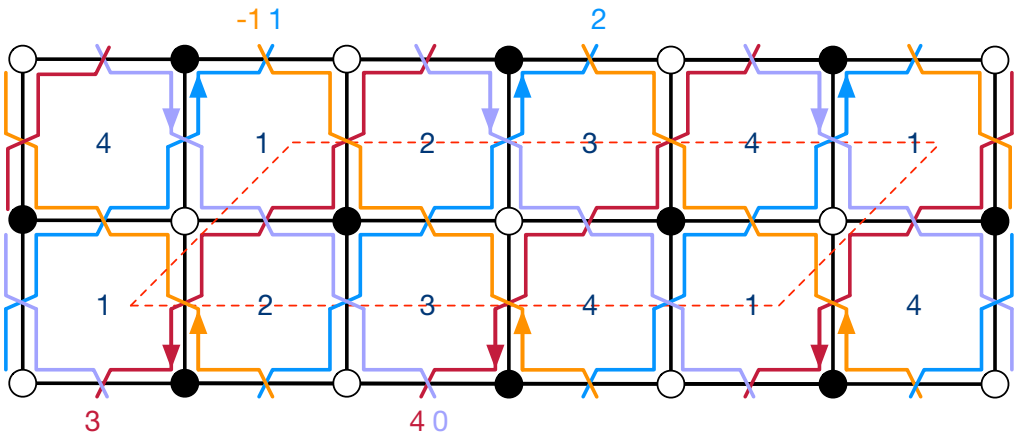

Figure 6. Brane tiling for the non-chiral $\mathbb{Z}_N$ orbifold of the conifold under consideration for the case $N = 2$. We show the zig-zag paths associated to the legs of the web in figure 5. Dashed red lines indicate the boundary of the unit cell.

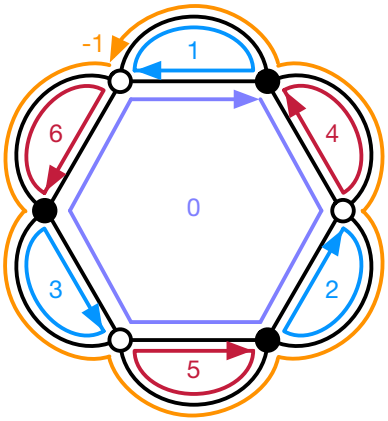

Figure 7. Bipartite graph on a sphere with $2N + 2$ punctures describing the twin quiver theory. The polygon at the center is a $2N$-gon. Here we show the case of $N = 3$.

explicitly indicated. The superpotential is quartic and can be easily read from figure 7. Below we write it for some explicit examples.

4.1 Conifold/$\mathbb{Z}_2$

For concreteness, let us consider the case of $N = 2$. The twin quiver is shown in figure 9.

The superpotential for the twin quiver can be read from the untwisted dimer, analogous to figure 7, and is

$$\begin{aligned} W = {} & X_{1,-1}X_{-1,4}X_{4,0}X_{0,1} + X_{3,0}X_{0,2}X_{2,-1}X_{-1,3} \\ & - X_{0,1}X_{1,-1}X_{-1,3}X_{3,0} - X_{-1,4}X_{4,0}X_{0,2}X_{2,-1}\,. \end{aligned} \tag{4.1}$$

From figure 9, it is clear that there are two qualitatively different possible mutations: either mutating one of the $-1, 0$ nodes, or mutating one of the $1, \ldots, 4$ nodes. Let us consider each case in further detail.

JHEP10(2024)118

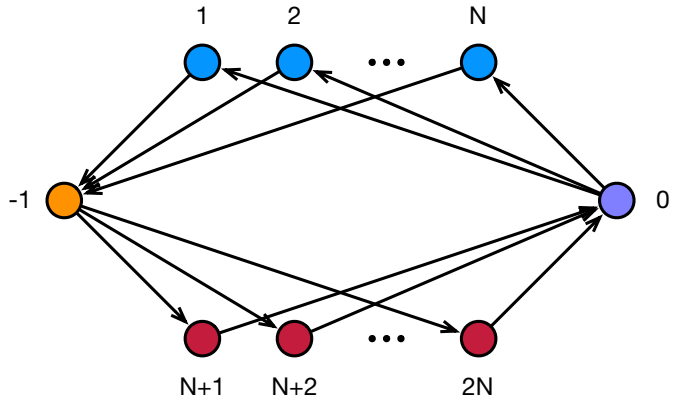

Figure 8. Twin quiver for a non-chiral $\mathbb{Z}_N$ orbifold of the conifold, which corresponds to N^2 free hypermultiplets in $5d$.

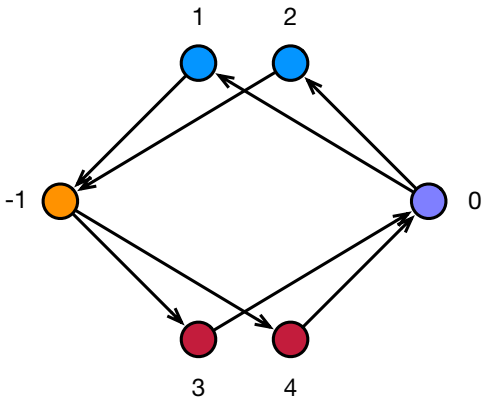

Figure 9. Twin quiver for a non-chiral $\mathbb{Z}_2$ orbifold of the conifold, which corresponds to 4 free hypermultiplets in $5d$.

Mutating 1. As it is customary, let us denote the number of colors of the (unitary) gauge groups by N_c and the number of flavors (i.e. either the number of incoming or outgoing chiral arrows at a given node) by N_f. Since node 1 has $N_f = N_c = 1$, it disappears upon mutation. As a consequence, there are no magnetic quarks. There is only one new field in the quiver, the meson $X_{0,-1}$, which, in terms of fields in the theory before the mutation, corresponds to the composition $X_{0,1}X_{1,-1}$. The resulting quiver is shown on the left panel of figure 11. It indeed corresponds to the brane web on the right of figure 11, which was obtained from the one in figure 5 by the brane crossing shown in figure 10. We will perform similar brane crossings in the other examples considered in this paper.

The superpotential follows from the mutation rules and is

$$\begin{aligned} W = {} & X_{0,-1}X_{-1,4}X_{4,0} + X_{3,0}X_{0,2}X_{2,-1}X_{-1,3} \\ & - X_{0,-1}X_{-1,3}X_{3,0} - X_{-1,4}X_{4,0}X_{0,2}X_{2,-1}\,. \end{aligned} \tag{4.2}$$

It is interesting to perform one further mutation on node 3. Once again, $N_f = N_c = 1$ for the mutated node, so it disappears upon mutation. The new meson is $Y_{-1,0} = X_{-1,3}X_{3,0}$.

JHEP10(2024)118

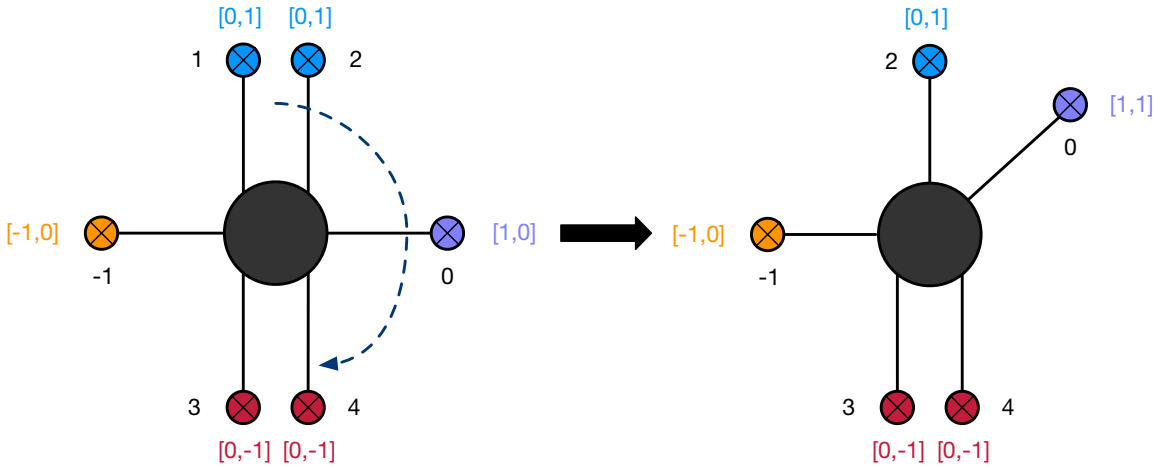

Figure 10. Brane crossing connecting figure 5 to figure 11.

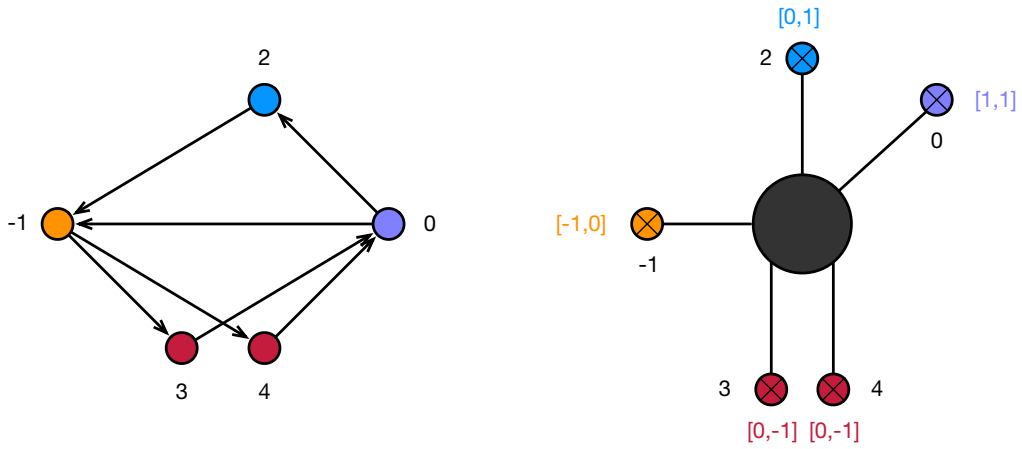

Figure 11. Quiver and web after mutating node 1 in figure 9.

The superpotential is given by

$$W = X_{0,-1}X_{-1,4}X_{4,0} + X_{0,2}X_{2,-1}Y_{-1,0} - X_{0,-1}Y_{-1,0} - X_{-1,4}X_{4,0}X_{0,2}X_{2,-1}\,. \tag{4.3}$$

Integrating out the massive fields $X_{0,-1}$ and $Y_{-1,0}$, we obtain the quiver in figure 12 and the superpotential vanishes.[19] As expected, this twin quiver is the one associated to crossing upwards one of the red 7-branes in the web on the left panel of figure 11. Finally, we can directly obtain this twin quiver starting from the dimer in figure 7 for the $N = 1$ case.

Mutating −1. This node has $N_f = 2N_c = 2$. As a result, the rank of node -1 is still 1 after the mutation. The twin quiver and web after the mutation are shown in figure 13 below.

[19] More precisely, the untwisted dimer (as the original one) has two vertices of order 4. Those two vertices would correspond to two quartic terms involving the same fields, but in different order. Since the twin quiver under consideration is Abelian, the ordering does not matter and the two terms cancel each other. The structure of the superpotential can also be determined using the construction in section 2.3.

JHEP10(2024)118

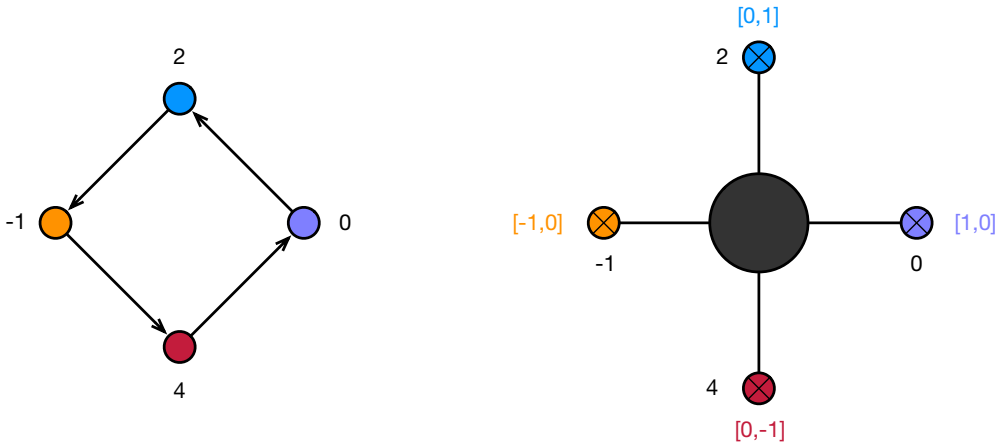

Figure 12. Quiver and web after mutating nodes 1 and 3 in figure 9.

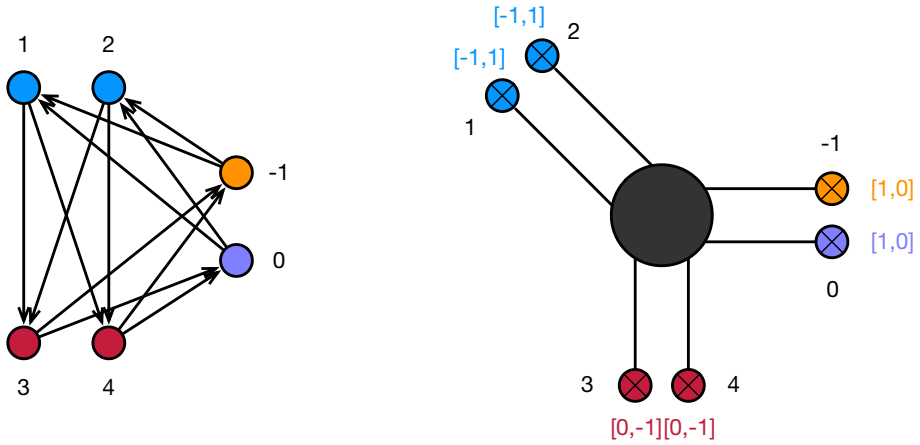

Figure 13. Quiver and web after mutating node -1 in figure 9.

They correspond to the so-called T_2 theory. The superpotential is

$$W = X_{1,4}X_{4,0}X_{0,1} + X_{3,0}X_{0,2}X_{2,3} - X_{0,1}X_{1,3}X_{3,0} - X_{4,0}X_{0,2}X_{2,4} \\ +X_{-1,1}X_{1,3}X_{3,-1} - X_{-1,1}X_{1,4}X_{4,-1} - X_{-1,2}X_{2,3}X_{3,-1} + X_{-1,2}X_{2,4}X_{4,-1}\,. \tag{4.4}$$

5 Multiple toric phases, a first encounter

The alert reader might notice that the starting point of our analysis in section 4 was rather arbitrary. In particular, the $\mathbb{Z}_N$ orbifold of the conifold has multiple toric phases for $N > 1$, and the brane tiling in figure 6 is just one of them. The toric phase described by figure 6 is "minimal", in the sense of having the minimum number of chiral fields and being obtained by combining copies of the conifold brane tiling. However, it is natural to ask how the results of the previous section are affected by starting from a different phase.

For concreteness, let us continue with the case of $N = 2$. This geometry has only two toric phases, up to relabeling of the nodes. One of them is the one we have previously

JHEP10(2024)118

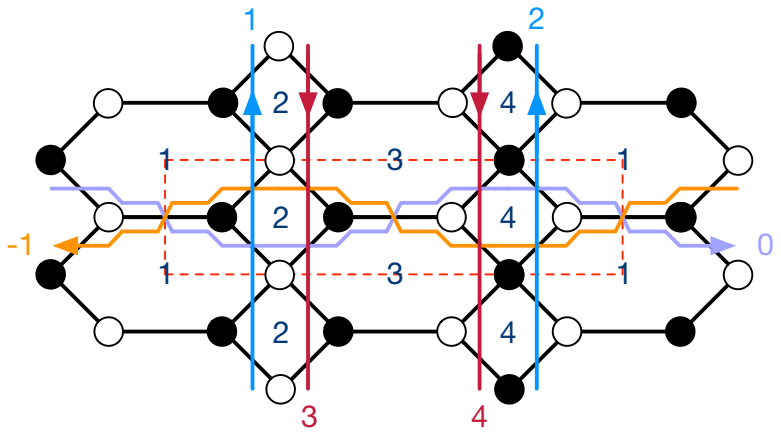

Figure 14. Brane tiling for another toric phase of the non-chiral $\mathbb{Z}_2$ orbifold of the conifold under consideration. We show the zig-zag paths associated to the legs of the web in figure 5.

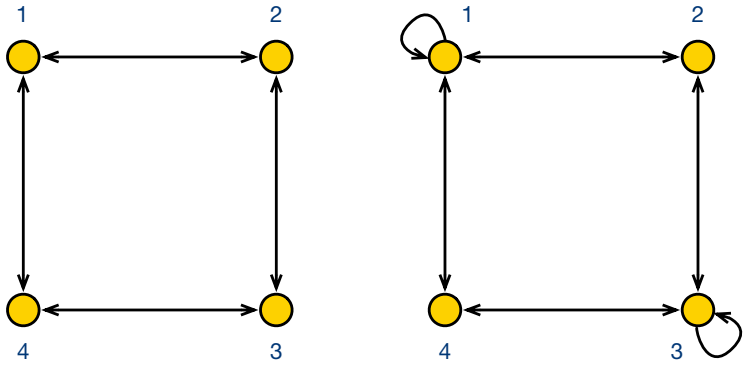

Figure 15. Original quivers for the two toric phases of the non-chiral $\mathbb{Z}_2$ orbifold of the conifold under consideration. They are connected by Seiberg duality on either node 2 or 4. Mutating node 1 or 3 of the first quiver leads to equivalent results.

considered, which is given by figure 6, while the new one is described by the brane tiling in figure 14. Figure 15 shows the corresponding quiver.

Let us now repeat the analysis of section 4.1, but using the toric phase in figure 14 as the starting point. Untwisting leads to the twin quiver defined by the bipartite graph in figure 16. As expected, the graph lives on a sphere with 6 punctures. However, it differs from the $N = 2$ case of the graph shown in figure 7. On the right of the figure, we show the corresponding quiver.

The difference between the twin quivers in figures 9 and 16 is the presence of bidirectional arrows.[20] This could have been in no other way, since the antisymmetric part of the adjacency matrix can be determined from the web in figure 5 and must be the same. The superpotential

[20]The two theories, of course, also differ in the superpotentials. These can be read off the corresponding bipartite graphs.

JHEP10(2024)118

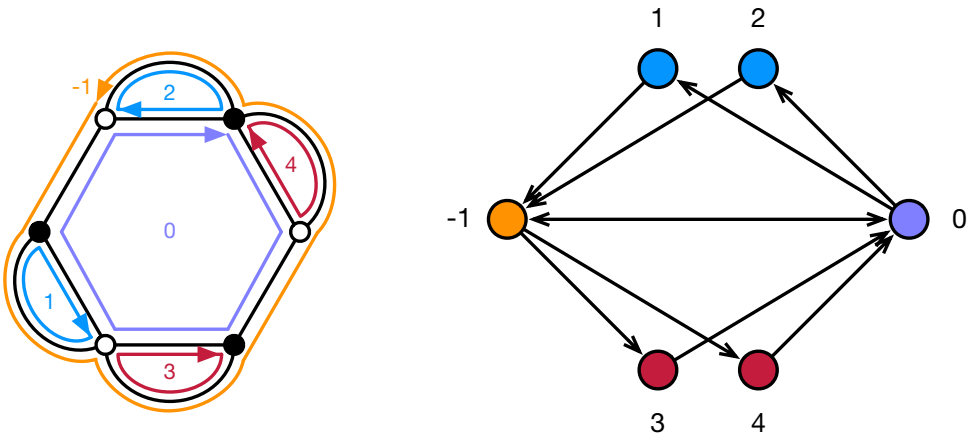

Figure 16. Untwisted dimer and corresponding twin quiver for the second phase of the non-chiral $\mathbb{Z}_2$ orbifold of the conifold associated to 4 free hypermultiples in $5d$.

for the twin quiver is

$$\begin{aligned} W = & X_{-1,0}X_{0,1}X_{1,-1} + X_{-1,3}X_{3,0}X_{0,-1} + X_{-1,4}X_{4,0}X_{0,2}X_{2,-1} \\ & - X_{-1,3}X_{3,0}X_{0,1}X_{1,-1} - X_{-1,0}X_{0,2}X_{2,-1} - X_{-1,4}X_{4,0}X_{0,-1}\,. \end{aligned} \tag{5.1}$$

Below, we study the mutations of the web. As before, we have two qualitatively different possibilities.

Mutating 1. Let us mutate the twin quiver on any of the blue or red nodes in figure 16. Without loss of generality, we can assume it is node 1. Since the extra bidirectional arrow is not connected to node 1, the mutation is qualitatively similar to the previous case. Once again, since $N_f = N_c = 1$, node 1 disappears in the mutation. There is a new meson $Y_{0,-1} = X_{0,1}X_{1,-1}$ and the superpotential is given by

$$\begin{aligned} W = & Y_{0,-1}X_{-1,0} + X_{-1,3}X_{3,0}X_{0,-1} + X_{-1,4}X_{4,0}X_{0,2}X_{2,-1} \\ & - X_{-1,3}X_{3,0}Y_{0,-1} - X_{-1,0}X_{0,2}X_{2,-1} - X_{-1,4}X_{4,0}X_{0,-1}\,. \end{aligned} \tag{5.2}$$

Figure 17 shows the mutated twin quiver.

From the superpotential (5.3), we see that the fields $Y_{0,-1}$ and $X_{-1,0}$ in the bidirectional arrow are massive. Integrating them out, we remove the bidirectional arrow from the quiver and the superpotential becomes

$$\begin{aligned} W = & X_{-1,3}X_{3,0}X_{0,-1} + X_{-1,4}X_{4,0}X_{0,2}X_{2,-1} \\ & - X_{-1,3}X_{3,0}X_{0,2}X_{2,-1} - X_{-1,4}X_{4,0}X_{0,-1}\,. \end{aligned} \tag{5.3}$$

This is precisely the theory in figure 11, upon the relabeling of nodes $3 \leftrightarrow 4$.

Mutating -1. Things become more interesting when we mutate node -1 (or equivalently node 0), since the additional bidirectional arrow increases its number of flavors. Indeed, node -1 has $N_f = 3N_c = 3$ and it therefore becomes a U(2) gauge group after mutation. The

JHEP10(2024)118

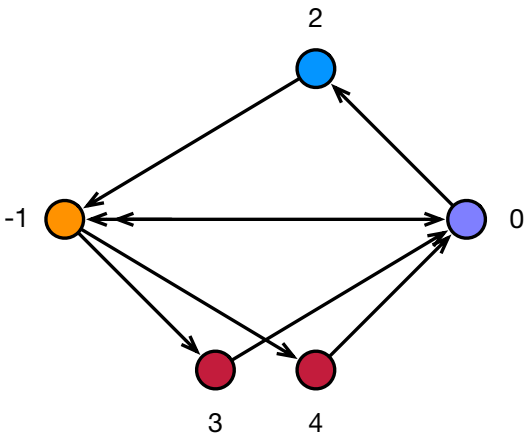

Figure 17. Quiver after mutating node 1 in figure 16. A pair of arrows connecting nodes 0 and -1 in opposite directions are massive and can be integrated out.

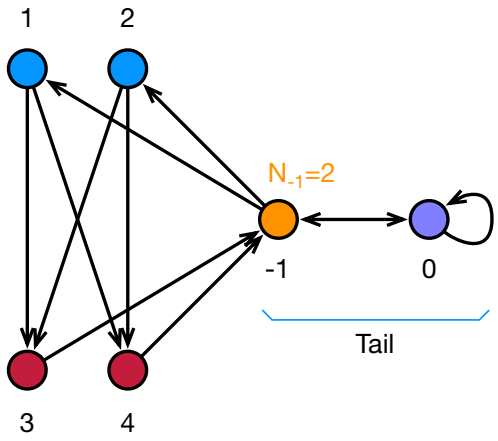

Figure 18. Quiver obtained by mutating figure 16 on node -1. This example contains a quiver tail.

incoming fields $X_{A,-1}$ ($A = \{0,1,2\}$) combine with the outgoing ones $X_{-1,a}$ ($a = \{0,3,4\}$) to form mesons $M_{A,a} = X_{A,-1}X_{-1,a}$. Finally, we denote the magnetic quarks $Y_{-1,A}$ and $Y_{a,-1}$. The resulting superpotential is

$$\begin{aligned} W \;=\; & X_{0,1}M_{1,0} + X_{3,0}M_{0,3} + X_{4,0}X_{0,2}M_{2,4} \\ & -X_{3,0}X_{0,1}M_{1,3} - X_{0,2}M_{2,0} - X_{4,0}M_{0,4} + Y_{-1,A}M_{A,a}Y_{a,-1}\,. \end{aligned} \tag{5.4}$$

The fields $X_{0,1}$, $X_{0,2}$,$X_{3,0}$, $X_{4,0}$, $M_{1,0}$, $M_{2,0}$, $M_{0,3}$ and $M_{4,0}$ are massive. Integrating them out, we obtain the quiver in figure 18, whose superpotential is

$$\begin{aligned} W \;=\; & Y_{0,-1}Y_{-1,0}M_{0,0} - Y_{-1,0}Y_{0,-1}Y_{-1,1}M_{1,3}Y_{3,-1} + Y_{-1,0}Y_{0,-1}Y_{-1,2}M_{2,4}Y_{4,-1} \\ & +M_{1,3}Y_{3,-1}Y_{-1,1} + M_{2,3}Y_{3,-1}Y_{-1,2} + M_{1,4}Y_{4,-1}Y_{-1,1} + M_{2,4}Y_{4,-1}Y_{-1,2}\,. \end{aligned} \tag{5.5}$$

The twin quiver in figure 18 exhibits an interesting structure, which we will denote *quiver tail*. Node 0 contains an adjoint and is connected to node -1 by a bidirectional arrow. Moreover, the ranks of the nodes decrease along the tail.

JHEP10(2024)118

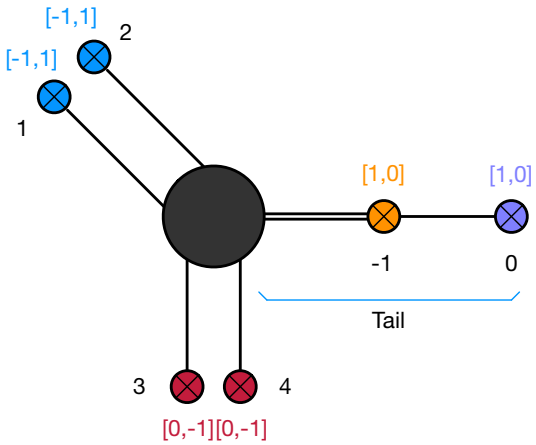

Figure 19. Brane web associated to the twin quiver with a tail in figure 18.

What does the tail in the twin quiver represent for the corresponding brane web? We claim that its natural interpretation is given by figure 19. This web is a particular mass deformation of the one in figure 13, in which masses are tuned such that two 7-branes are aligned so the corresponding 5-branes can split into segments while respecting the s-rule. The existence of the quiver tail can be traced to the fact that we started from a different toric phase for the underlying geometry. This suggests that different toric phases of the original theory allow to capture the roots of the Higgs branch in the extended Coulomb branch of the associated $5d$ theory. In what follows, we will investigate this proposal in further detail.

5.1 Extended Coulomb branch, toric phases and twin quivers

Given the toric diagram Δ of a toric CY_3 fold $\mathcal{M}$ the mirror partner $\mathcal{W}$ can be constructed as follows [49]. We introduce the Newton polynomial

$$P(x,y) = \sum_{(m,n)\in\Delta\cap\mathbb{Z}^2} c_{(m,n)} x^m y^n \,, \tag{5.6}$$

which contains a term for every point in Δ and where the $c_{(m,n)}$ are complex coefficients. Three of these coefficients can be set to 1 by rescaling x, y, and an overall $\mathrm{SL}(2,\mathbb{Z})$ transformation.[21]

The mirror geometry is a double fibration over a complex plane $\mathbb{C}$ parametrized by w as[22]

$$\mathcal{W} = \begin{cases} P(x,y) = w \,, \\ uv = w \,. \end{cases} \tag{5.7}$$

The $5d$ theory and its BPS quiver are encoded in the Riemann surface Σ corresponding to the fiber at $w = 0$, namely defined by

$$P(x,y) = 0 \,. \tag{5.8}$$

[21] Going from ordinary toric diagrams to GTPs with white dots, corresponds to freezing some of these moduli by further constraining the coefficients in the Newton polynomial [50].

[22] Strictly speaking, this construction is restricted to Δ's with at least one internal point.

JHEP10(2024)118

The *coamoeba* projection of Σ corresponds to the following projection onto a 2-torus

$$(x, y) \to (\arg x, \arg y)\,, \tag{5.9}$$

Mirror symmetry provides an algorithmic prescription for constructing the toric phase for every point in the extended Coulomb branch, namely for every choice of coefficients in the Newton polynomial. For every such point, the corresponding brane tiling is determined by the coamoeba projection. These ideas were introduced in the seminal work [42], to which we refer the reader for further details. Every toric phase can be generated in this way, with different ones related by geometric transitions in the mirror [42, 51]. In turn, as previously discussed, the corresponding twin quivers are obtained by untwisting.

In turn, the *amoeba* projection of Σ onto $\mathbb{R}^2$, defined as

$$(x, y) \to (\log|x|, \log|y|)\,, \tag{5.10}$$

is a thickened version of the brane web. The different parameters of the web are controlled by combinations of the coefficients in the Newton polynomial.

5.2 Tail decoupling, GTPs and node merging

Motivated by the previous results, let us investigate how twin quivers capture other transformations of the corresponding webs. Let us strip off the tail in figure 19. To do so, we turn on a non-zero VEV for the adjoint in figure 18.[23] This corresponds to entering the Higgs branch by sliding out of the plane the segment between nodes -1 and 0 in figure 19. Plugging this VEV into the superpotential (5.5) makes the pair of bifundamental fields extended between nodes -1 and 0 massive, effectively decoupling node 0 from the rest of the quiver. This operation corresponds to sliding the 5-brane segment that stretches between the 7-branes -1 and the 0 along them to infinity. The superpotential becomes

$$W = M_{1,3}Y_{3,-1}Y_{-1,1} + M_{2,3}Y_{3,-1}Y_{-1,2} + M_{1,4}Y_{4,-1}Y_{-1,1} + M_{2,4}Y_{4,-1}Y_{-1,2}\,. \tag{5.11}$$

Figure 20 shows the web after decoupling the tail. It contains two 5-brane legs that terminate on a single 7-brane, i.e. it corresponds to a GTP with a white dot, as shown in the same figure. Then, it should be possible to alternatively construct the corresponding twin quiver using the algorithm discussed section 2.3 including its third step, i.e. node merging. It is straightforward to verify that merging nodes -1 and 0 of the quiver in figure 13 into a single rank-2 node produces the desired quiver. Implementing the identification of nodes in the superpotential results in

$$\begin{aligned} W = {} & X_{1,4}(\tilde{X}_{4,-1}\tilde{X}_{-1,1} + X_{4,-1}X_{-1,1}) + X_{2,3}\tilde{X}_{3,-1}(\tilde{X}_{-1,2} + X_{3,-1}X_{-1,2}) \\ & + X_{1,3}(\tilde{X}_{3,-1}\tilde{X}_{-1,1} + X_{3,-1}X_{-1,1}) + X_{2,4}(\tilde{X}_{4,-1}\tilde{X}_{-1,2} + X_{4,-1}X_{-1,2})\,. \end{aligned} \tag{5.12}$$

where we have assumed generic coefficients for each monomial and combined the bifundamentals connected to the merged nodes into doublets. Upon obvious relabeling, both the quiver and the superpotential (5.12) agree with the ones we previously derived by removing the tail.

[23] More precisely, this field is an "adjoint" of a U(1) node, i.e. it is actually a singlet.

JHEP10(2024)118

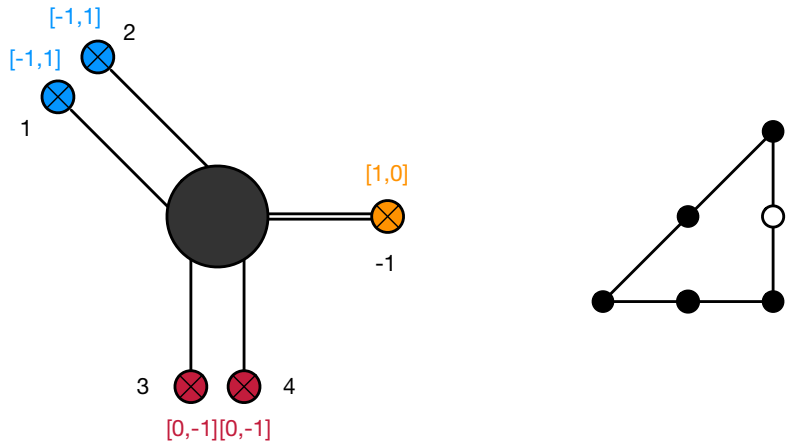

Figure 20. Brane web obtained from figure 19 by decoupling brane 0 and the corresponding GTP.

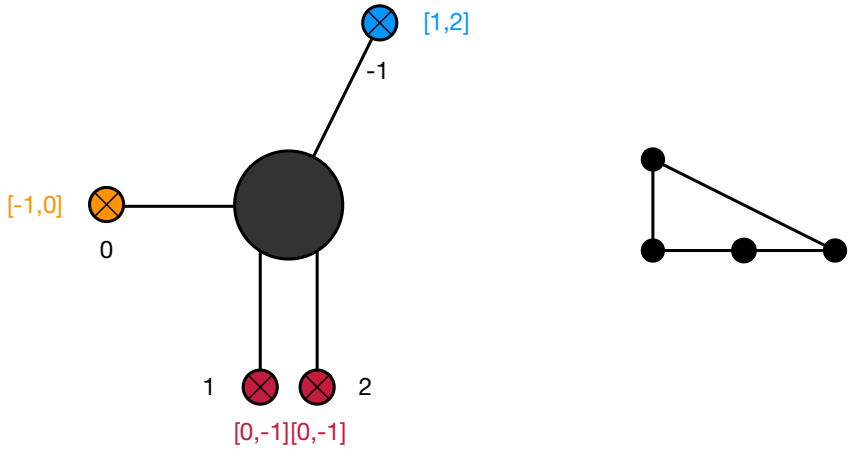

Figure 21. Brane web for "$\mathrm{SU}(1)_1$", i.e. a free hypermultiplet. It corresponds to $\mathbb{C}^2/\mathbb{Z}_2 \times \mathbb{C}$.

6 Additional examples

In section 5, we presented evidence that the different toric phases of the original theory allow to explore different chambers of the extended Coulomb branch of the $5d$ theory. This section contains additional examples that go beyond free theories, showing that this is a general phenomenon.

6.1 Revisiting the free hypermultiplet: self-dual webs

When the class of webs in figure 5 is specialized for $N = 1$ as in figure 12, it engineers a single free hypermultiplet in $5d$. Formally, this theory can be regarded as "$\mathrm{SU}(1)_0$". The web for "$\mathrm{SU}(1)_1$", shown in figure 21, provides an alternative realization of a free hypermultiplet.

This web is dual to the $\mathbb{C}^2/\mathbb{Z}_2 \times \mathbb{C}$ singularity. There is a single toric phase for D3-branes probing this geometry, whose brane tiling is shown in figure 22.

JHEP10(2024)118

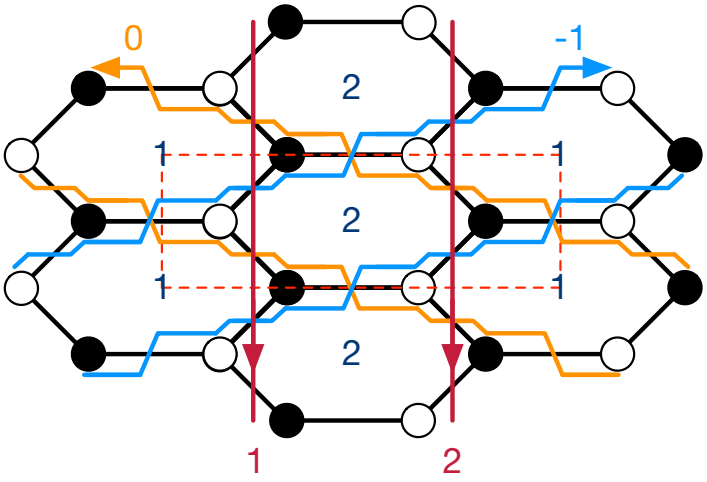

Figure 22. Brane tiling for $\mathbb{C}^2/\mathbb{Z}_2 \times \mathbb{C}$. We show the zig-zag paths associated to the legs of the web in figure 21.

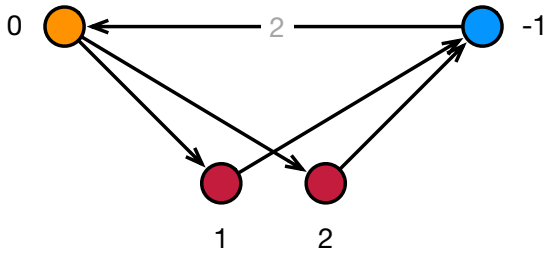

Figure 23. Twin quiver for figure 21.

Untwisting the brane tiling, we obtain the twin quiver shown in figure 23, whose superpotential is

$$W = X_{1,-1}Y_{-1,0}X_{0,1} + X_{-1,0}X_{0,2}X_{2,-1} - X_{0,1}X_{1,-1}X_{-1,0} - Y_{-1,0}X_{0,2}X_{2,-1}\,. \tag{6.1}$$

Crossing brane -1 in figure 21 results in the web shown figure 24. Interestingly, the initial and mutated webs are $\mathrm{SL}(2,\mathbb{Z})$ equivalent, therefore they describe the same $5d$ theory.

The observed self-duality is nicely captured by the twin quiver, which returns to itself when mutated on node -1 (up to relabeling nodes).

Finally, we note that upon crossing any of the red branes in figure 21, it decouples from the web. The same happens if one crosses any of the branes in figure 12. Both cases result in the same web, the one for $\mathbb{C}^3$. It is a straightforward to verify that the corresponding mutations of the twin quivers in figures 23 and 12 indeed result in the same quiver.

6.2 The rank 1 E_1 theory

Let us explore a full-fledged interacting $5d$ theory, the E_1 theory, whose web is shown in figure 25.

The four legs of the web are equivalent. Without loss of generality, let us consider crossing 7-brane 1 to the other side. Generically, we obtain the configuration on the left of

JHEP10(2024)118

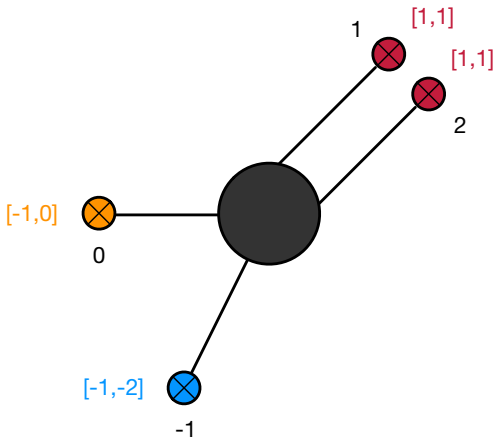

Figure 24. Crossing the blue 7-brane in 21.

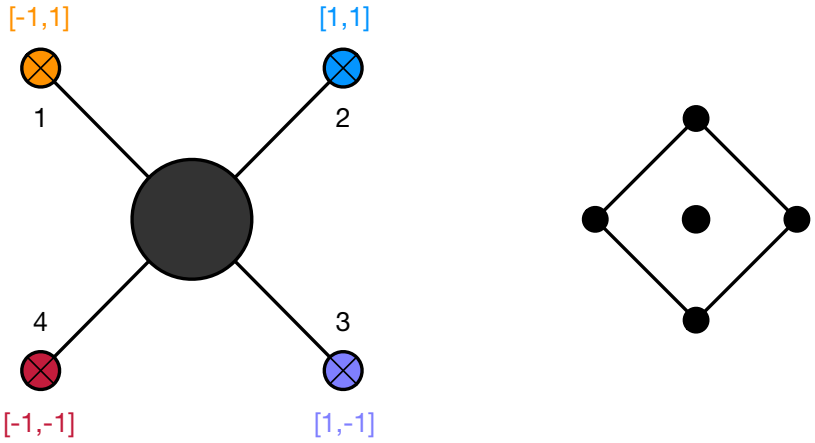

Figure 25. Brane web for the E_1 theory. The dual toric diagram corresponds to $\mathbb{F}_0$.

figure 26. However, in view of our previous experience, we expect the existence of another toric phase for the E_1 theory that results on a twin quiver associated to the root of the Higgs branch, shown on the right figure 26.

As shown in figure 25 the web for E_1 is dual to the toric diagram for $\mathbb{F}_0$. There are two toric phases for D3-branes probing this geometry [23, 52–54]. We present the corresponding brane tilings and quivers in figure 27.

Untwisting the brane tilings in figure 27, we obtain the twin quivers in figure 29 (see [42] for further details).

As expected, the two twin quivers differ by the presence of bidirectional arrows. Their superpotentials can be easily determined from the corresponding graphs. The extra arrows turn otherwise toric nodes, i.e. nodes with $N_f = 2N_c$, into non-toric ones. This agrees with the expectation from figure 26. Indeed, while it is straightforward to check that mutating any node — they are all equivalent — of phase 1 in figure 29 gives a quiver naturally associated to the web on the left of figure 26, mutating any node of phase 2 in figure 29 gives figure 30. The triangular sub-quiver consisting of the yellow, red and light blue nodes

JHEP10(2024)118

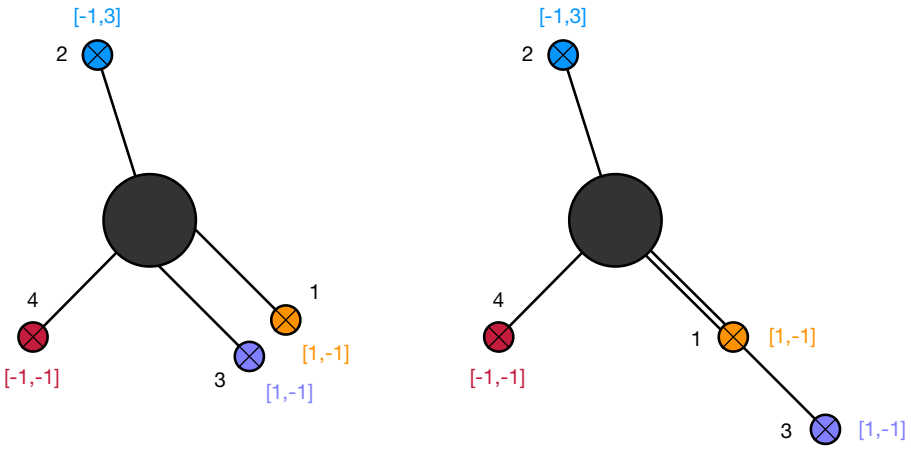

Figure 26. Brane webs obtained by crossing 7-brane 1 in the E_1 theory.

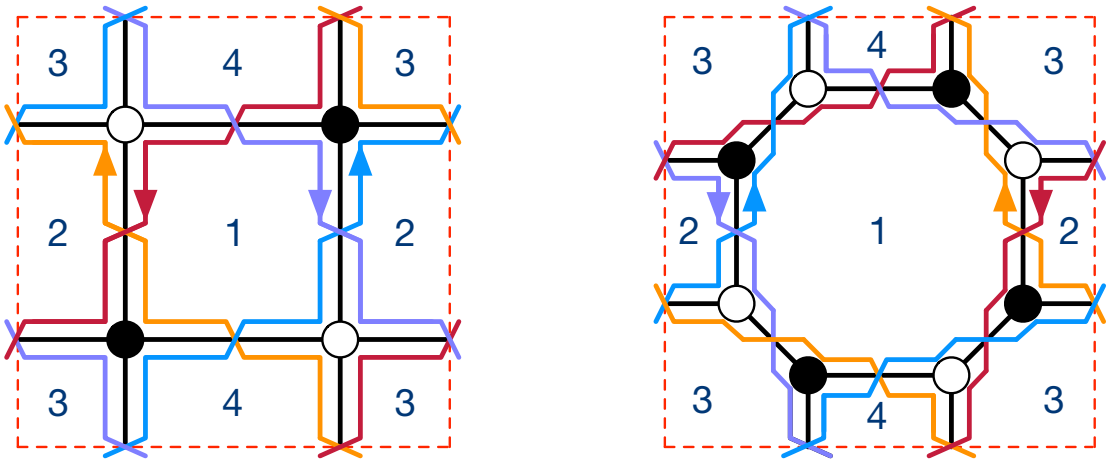

Figure 27. Brane tilings for the two toric phases of $\mathbb{F}_0$. We distinguish the zig-zags with the colors of the corresponding 7-branes in figure 25.

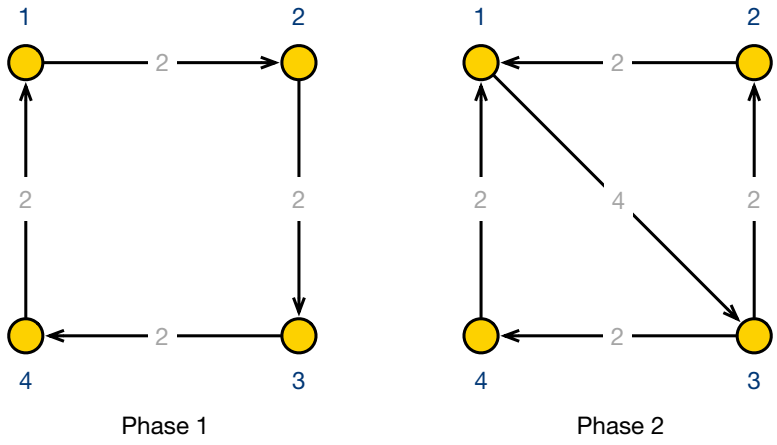

Figure 28. Original quivers for the two toric phases of $\mathbb{F}_0$.

JHEP10(2024)118

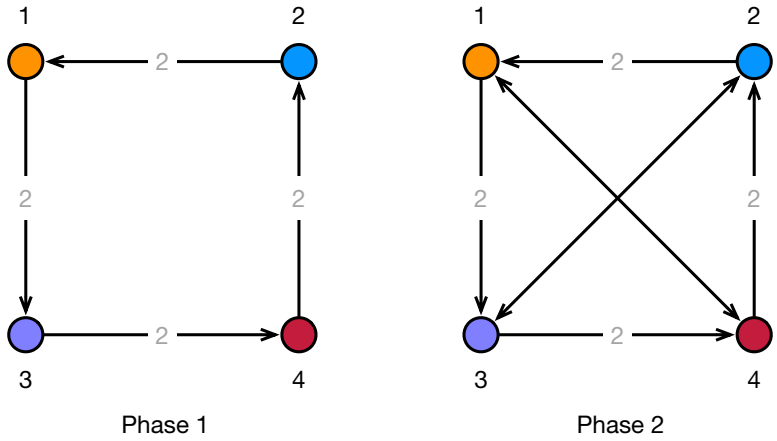

Figure 29. Twin quivers obtained from the two toric phases of $\mathbb{F}_0$.

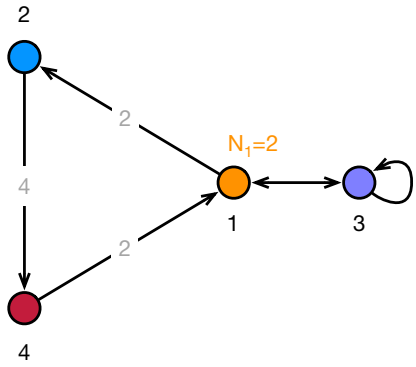

Figure 30. Mutating the twin quiver for phase 2 in figure 29 gives rise to a quiver tail. Here we show a mutation on node 1.

agrees with the corresponding sub-web on the right of figure 26. In addition, the tail of the twin quiver agrees with the web.

Similarly to the example in section 5.2, one can check that node merging in the mutation of phase 1 produces the same result as tail removal in the mutation of phase 2.

6.3 The E_2 theory

Let us now turn our attention to the E_2 theory, whose brane web is shown in figure 31.

Crossing the 7-brane 1 we obtain, generically, the web shown on the left of figure 32. Once again, there is a root of the Higgs branch in the extended Coulomb branch, whose web is shown on the right of figure 32.

As shown in figure 31, the E_2 web corresponds to the toric diagram for dP_2. There are two toric phases for D3-branes probing dP_2 [54]. As in previous examples, the webs in figure 32 can be related to these different phases. The brane tilings for the two toric phases of dP_2 and the BFTs obtained from them by untwisting were thoroughly discussed in [35], to where we refer the interested reader for details. Here we just present the two associated twin quivers, which are shown in figure 33. Once again, as anticipated, they only

JHEP10(2024)118

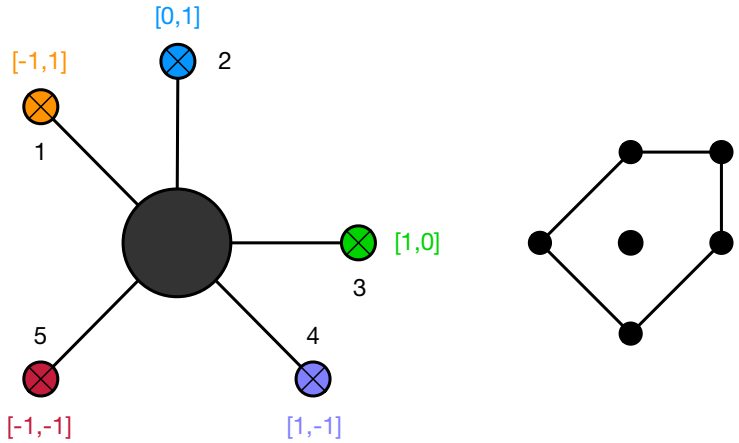

Figure 31. Brane web for the E_2 theory. The dual toric diagram corresponds to dP_2.

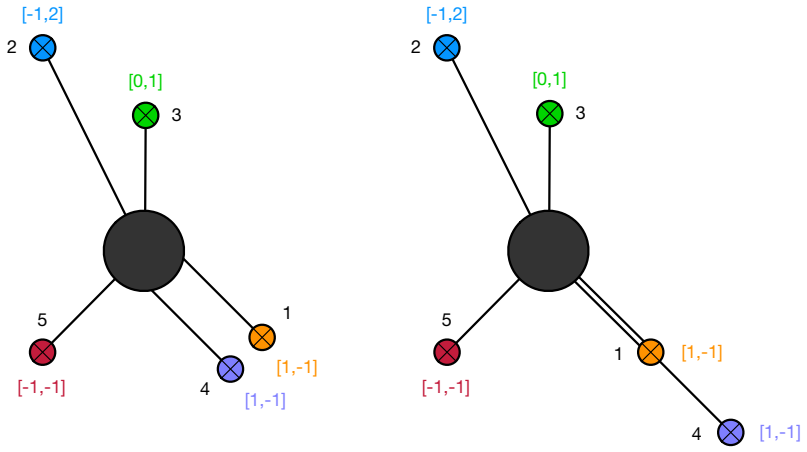

Figure 32. Brane webs obtained by crossing 7-brane 1 in the E_2 theory.

differ by bidirectional arrows, in this case stretched between nodes 1 and 4. As usual, it is straightforward to determine their superpotentials from the corresponding bipartite graphs.

We are interested in studying how the crossing of 7-brane 1 in figure 31 translates in terms of twin quivers. Based on our previous experience, we expect that the web containing a tail in figure 32 correspond to the dualization of the twin quiver for phase 2 in figure 33 on node 1. Performing the dualization, we obtain the quiver in figure 34, which nicely shows the tail. Moreover, it is easy to verify that the rest of the quiver is consistent with the right web in figure 32.

6.4 A larger example

In this section we present an additional example illustrating our ideas. Consider the web and associated toric geometry shown in figure 35. This theory was thoroughly investigated in [35], to where we refer the reader for further details.

Figure 36 shows two webs obtained by crossing 7-brane 6.

JHEP10(2024)118

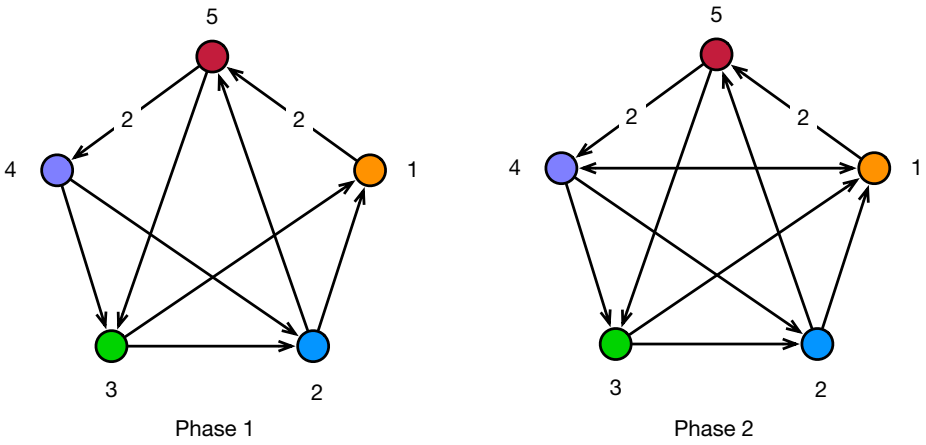

Figure 33. The two twin quivers for the E_2 theory, which come from the two toric phases of dP_2.

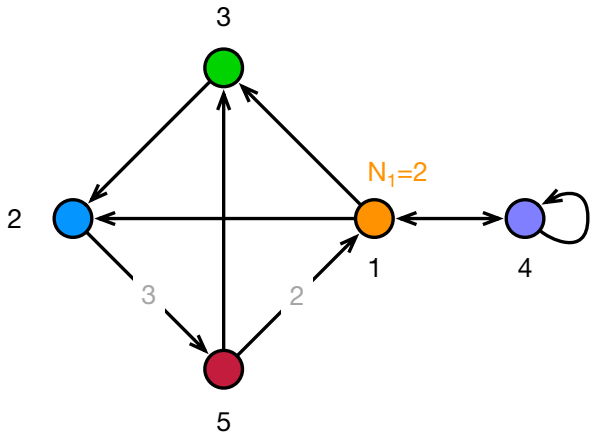

Figure 34. Mutation of the twin quiver for phase 2 in figure 33 on node 1.

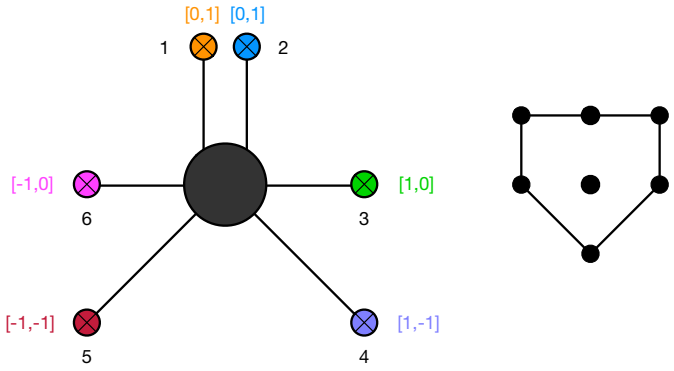

Figure 35. A brane web and its dual toric diagram.

JHEP10(2024)118

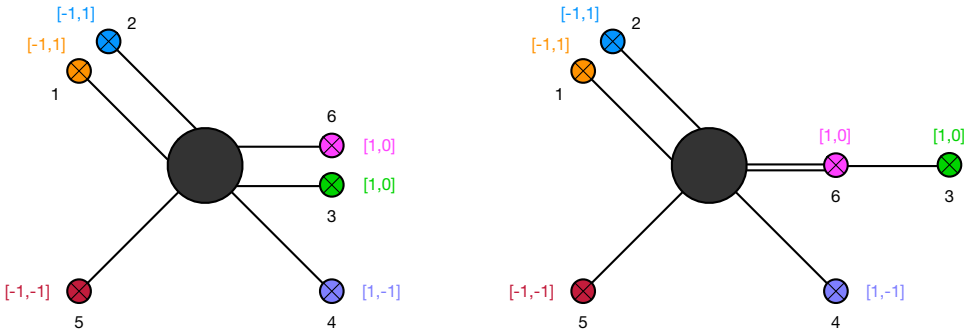

Figure 36. Brane webs obtained by crossing 7-brane 6 in figure 35.

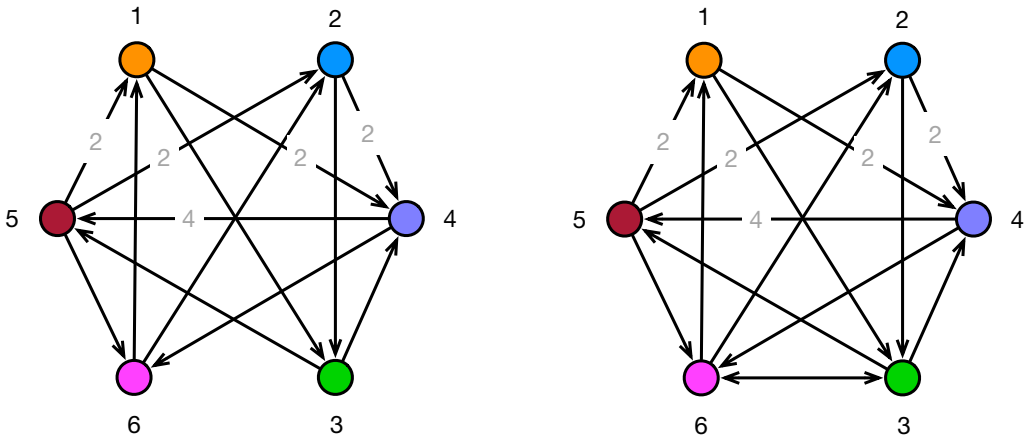

Figure 37. Two twin quivers for the geometry in figure 35.

Two twin quivers for the geometry in figure 35 were presented in [35].[24] We show them in figure 37.[25] They differ by the presence of bidirectional arrows between nodes 3 and 6, which correspond to anti-parallel legs in figure 35.

To obtain the quiver describing the web with a tail on the right of figure 35, we consider the mutation of the quiver on the right of figure 37 on node 6. The resulting quiver, shown in figure 38 exhibits the expected tail.

7 Towards general tails

We have presented evidence that the twin quivers constructed from different Seiberg dual phases of a given original theory capture different loci of the extended Coulomb branch of the $5d$ theory. Indeed, upon mutation, the twins of the different Seiberg dual phases exhibit tails which signal the root of a Higgs branch direction. Yet, the examples we have shown are restricted to cases where the Higgs branch direction captured by the tail is 1-dimensional, which follows from the fact that the twin quivers with a single bidirectional arrow before

[24]While we have not carried out an exhaustive classification of toric phases for this geometry, it is reasonable to expect additional ones exist. We do not consider this question any further, since twin quivers associated to other phases are not relevant for our discussion.

[25]The superpotential for both theories can be determined from the bipartite graphs presented in [35].

JHEP10(2024)118

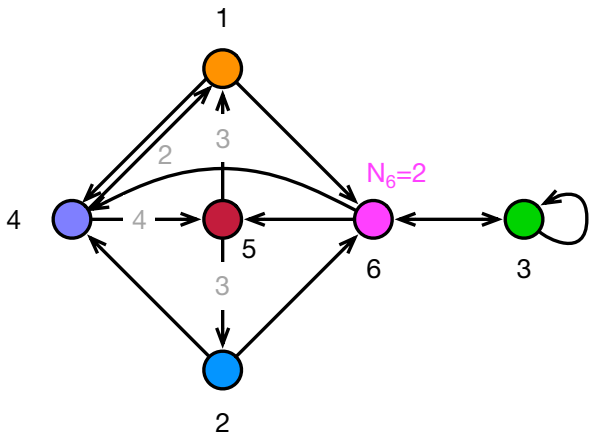

Figure 38. Mutation of the twin quiver on the right of figure 37 on node 6.

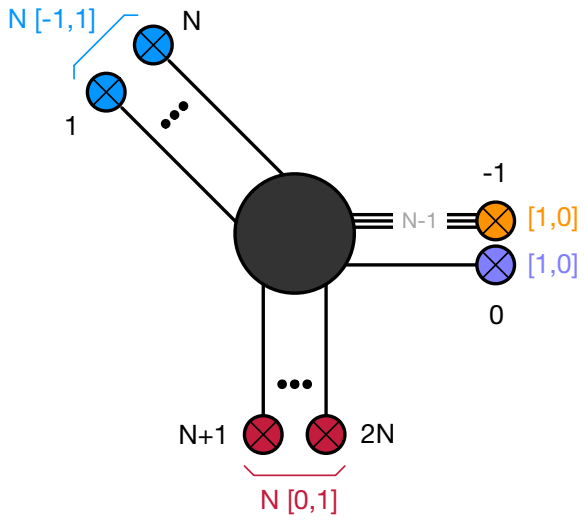

Figure 39. Web obtained by starting from figure 5 and moving brane -1 across the web.

the mutation that produces the quiver. It is natural to wonder whether this extends more generically to higher-dimensional Higgs branches. Related to this question, we would like to understand the general structure of tails arising from more than one bidirectional arrow between a given pair of nodes.

Rather than carrying out a general analysis, we will consider the class of models corresponding to the $\mathbb{Z}_N$ non-chiral orbifold of the conifold, whose web and toric diagrams were shown in figure 5. Moving brane -1 across the web, we obtain the configuration shown in figure 39. This web is nicely captured by the twin quiver obtained by mutating the one in figure 8 on node -1.

Generalizing the discussion for $N = 2$ in sections section 4 and section 5, the original theory for conifold/$\mathbb{Z}_N$ has various toric phases and that capture different loci in the extended Coulomb branch. It is straightforward to classify the toric phases for this geometry using Type IIA Hanany-Witten-type brane configurations, which are related to D3-branes probing the

JHEP10(2024)118

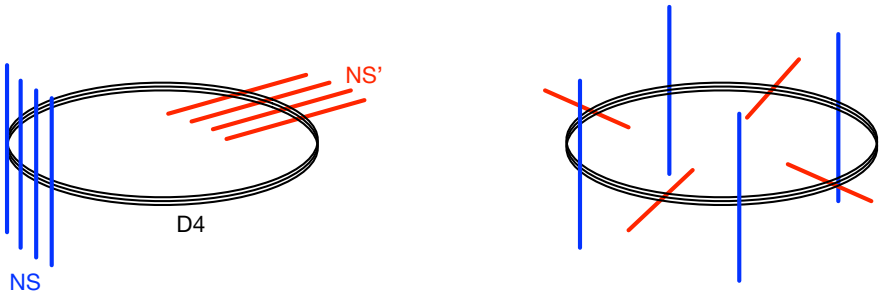

Figure 40. Type IIA configurations for conifold/$\mathbb{Z}_N$ (shown for $N = 4$). We show the configurations for two toric phases: one with 3 adjoints from parallel NS branes and 3 adjoints from parallel NS' branes (left) and one without adjoints (right).

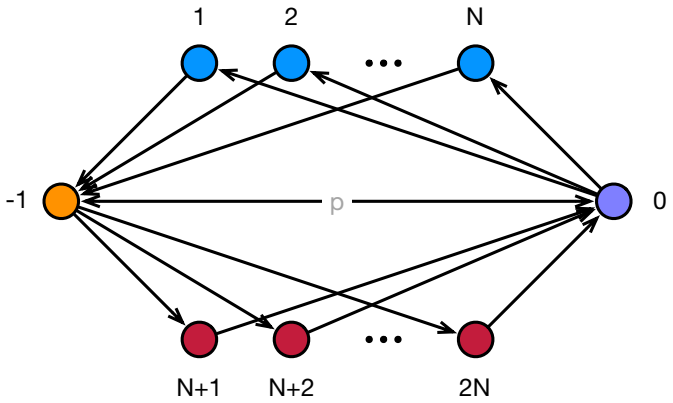

Figure 41. Twin quiver for a non-chiral $\mathbb{Z}_N$ orbifold of the conifold with p bidirectional arrows, where $0 \leq p \leq N-1$.

conifold/$\mathbb{Z}_N$ by T-duality [55]. The configurations consist of N NS5-branes in the (123456) directions, N orthogonal NS5'-branes along (123478) and D4-branes spanning (12346), with the 6 direction compactified on a circle. The different phases correspond to the possible arrangements of the NS and NS' branes on the circle with D4-branes, as shown in figure 40. Consecutive parallel NS or NS' branes correspond to nodes in the quiver with adjoints. Consequently, the number of adjoints coming from parallel NS or NS' branes ranges between 0 and $N-1$.

As in the conifold/$\mathbb{Z}_2$ example studied in section 5, pairs of adjoints turn into bidirectional arrows in the corresponding twin quivers obtained by untwisting. The twin quivers coming from different toric phases therefore have the general form shown in figure 41, which generalizes figure 8 by the bidirectional arrows. Following the discussion of the Hanany-Witten setups we conclude that there are N possible values for the number of bidirectional arrows p, given by $0 \leq p \leq N-1$. It is important to note that for $N > 2$ multiple toric phases can give rise to the same twin quiver, included the value of p, but that differ in the superpotential.

Following the discussion in previous sections, let us now considered a mutation on node -1 of the twin quiver. We obtain the quiver shown in figure 42, which illustrates the features of twin quivers with tails in more generic cases.

JHEP10(2024)118

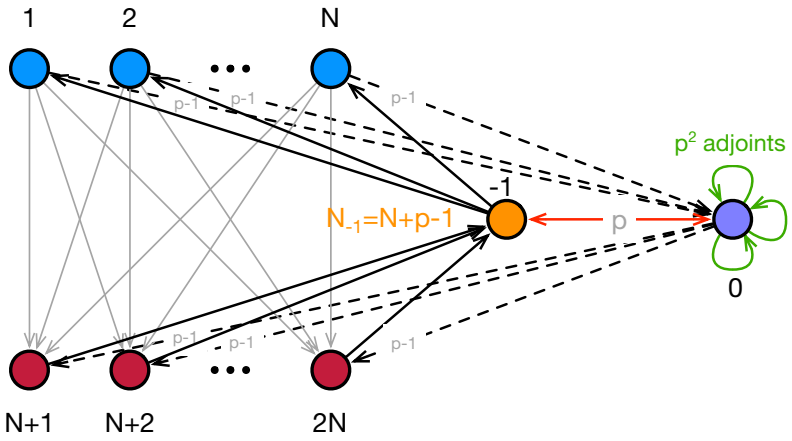

Figure 42. Twin quiver obtained by mutating node -1 in figure 41.

Let us discuss some of the main properties of this quiver. The ranks of all nodes are equal to 1, with the exception of node -1, whose rank is $N + p - 1$. We have used different colors to distinguish the matter fields:

- Black arrows are obtained by flipping the ones that connected node -1 to the blue and red ones.
- Grey arrows connect every node in the top layer (blue) to every node in the bottom layer (red). These fields are mesons (i.e. composite arrows) created by the mutation and have cubic couplings to the appropriate black arrows.
- There are still p bidirectional arrows, shown in red, connecting nodes -1 and 0.
- Node 0 has p^2 adjoints, which are shown in green. By adjoints, we actually mean arrows that start and end on the same node. Since node 0 is U(1), these fields are actually gauge singlets. These fields are also mesons and have cubic couplings, generated by the mutation, to the red fields.
- The dotted arrows are additional mesons generated by the mutation on node -1. In the case $p \geq 1$, for each red and blue node, one of these mesons pairs with the preexisting arrow in the opposite direction and become massive, resulting in $p - 1$ massless fields. The dotted arrows are not present for $p = 1$ and have the opposite orientation for $p = 0$.

We see that the familiar structure of the tail emerges in the generic case. Yet, depending on p it shows distinctive features. For example, for $p > 1$ the rank of node -1 becomes larger than N and new dotted arrows arise. The latter fact is suggestive of a web interpretation where extra 5-branes crossing the original web and attached to node -1 are superimposed. Since the web interpretation of these cases is less transparent, we will leave it as an open problem.

Thoughts on tail decoupling.

In section 5.2 we introduced a simple operation on the twin quiver that results in the decoupling of the tail and leaves behind the quiver for a GTP for the case of $p = 1$. It is natural to ask

JHEP10(2024)118

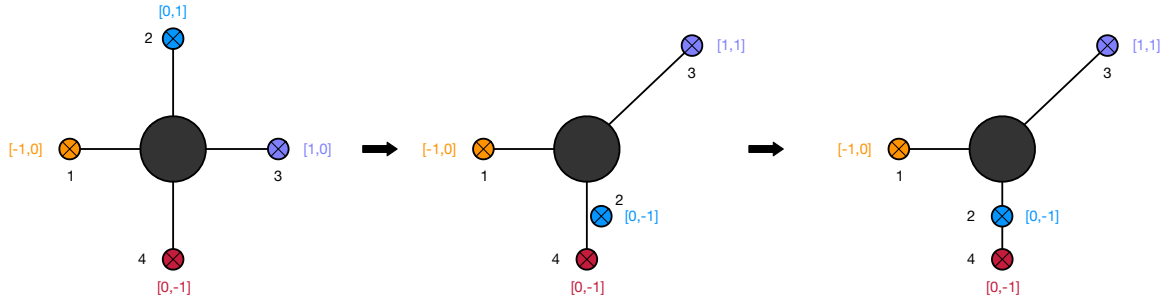

Figure 43. Web for 1 free hyper and its Higgs branch.

whether a similar decoupling at the level of the quiver exists for general values of p. Currently, we do not have an answer to this interesting question and we would like to emphasize that such a process might not even exist. However, we would like to collect a few thoughts on how we envision the quiver in figure 42 can potentially accommodate the decoupling:

- Turning on generic VEVs for the p^2 adjoint fields would generate masses for all the red fields. As a result, both the green and red arrows would disappear.
- As mentioned earlier, p can take values in the range $0 \leq p \leq N-1$, which agrees with the possible numbers of white dots in the corresponding edge of the GTP. Moreover, as mentioned earlier, there are various toric phases that lead to the twin quiver in figure 41 with the same value of p but different superpotential. It is tempting to speculate that, upon decoupling, these multiple quivers correspond to the different ways of distributing p white dots along a length N edge of the GTP.
- The process would need to be accompanied by a higgsing of node -1 that not only splits it into different nodes but also reduces the total rank.
- Finally, to fully decoupled node 0, it would be also be necessary for the dotted arrows to become massive. Optimistically, this could occur as a consequence of the higgsing in the previous point.

8 Tails as building blocks

We now discuss a puzzle that arises in the quiver description of certain brane configurations and propose a solution. The problem is rather generic but, for concreteness, we illustrate it with an example. Consider the web for a free hypermultiplet shown in figure 43.[26] Let us now cross one of the 7-branes. Without loss of generality, we can assume it is brane 2. In this process, brane 2 decouples from the rest of the web and can be moved away to infinity. This process is nicely captured by the twin quiver in figure 13, from which the corresponding node disappears after mutating it. However, as shown in figure 43, we can deal with brane 2 in a different way. Instead of sending it to infinity, we move it on top of the external leg that terminates on brane 4, splitting it. We recognize the resulting configuration as a tail.

[26]This is the same web in figure 12. For simplicity, we have labeled the 7-branes differently.

JHEP10(2024)118

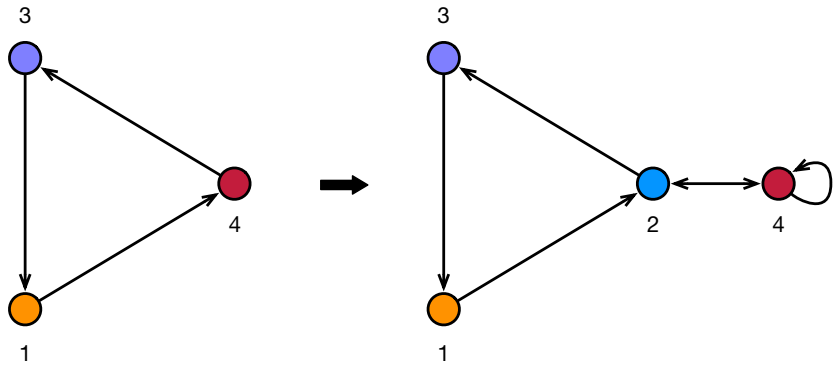

Figure 44. Left: the twin quiver associated to the connected component of the web at the center of figure 43. Right: we propose the twin quiver for the web on the right pf figure 43 is obtained by appending a tail.

The previous discussion raises a puzzle. The starting web in figure 43 corresponds to the conifold, which has a single toric phase. This results in a unique twin quiver, the one in figure 12. Contrary to previous examples, there is no extra toric phase from which we could obtain an alternative twin quiver by untwisting that, in turn, would give rise to the tail when the node associated to brane 2 is mutated. In short, there does not seem to be a twin quiver capable of reproducing the last step in figure 43.

We propose to construct the corresponding twin quiver by appropriately appending a tail, as shown in figure 44. In this case, in accordance with the web in figure 43, the rank of node 2 at the "root" of the quiver tail is 1. This quiver is certainly consistent with the basic properties of the web in figure 43, but what about the superpotential? Based on the symmetries of the configuration, it is natural to conjecture that

$$W = X_{4,4}X_{4,2}X_{2,4} + X_{2,3}X_{3,1}X_{1,2}X_{2,4}X_{4,2}\,. \tag{8.1}$$

We can test this proposal by mutating the quiver on node 2, which corresponds to taking brane 2 back to its original position. The resulting quiver is given in figure 45 below, and its superpotential is

$$W = X_{1,3}X_{3,2}X_{2,1} + X_{3,1}X_{1,4}X_{4,3} + X_{2,4}X_{4,3}X_{3,2} + X_{4,2}X_{2,1}X_{1,4}\,. \tag{8.2}$$

This result supports our proposal, since we obtained a natural extension of figure 12 by the addition of bidirectional arrows, with a superpotential that respects the symmetry of the web on the left of figure 43.

9 Conclusions

Twin quivers were introduced in [35] as new tools for studying the general class of $5d$ SCFTs encoded in webs of 5- and 7-branes or, equivalently, GTPs. In this paper we investigated the non-uniqueness of twin quivers that follows from the multiplicity of toric phases for a given toric Calabi-Yau 3-fold used in their construction. This phenomenon exists even for brane webs associated to ordinary toric diagrams, i.e. it is independent from the presence of white

JHEP10(2024)118

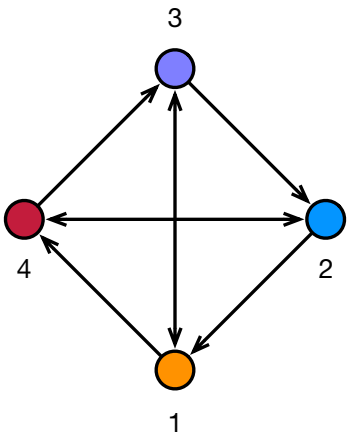

Figure 45. Mutation of the quiver on the right of figure 44 on node 2.

dots in GTPs. As noted in [35], twin quivers originating from different toric phases differ by bidirectional arrows. We found that such bidirectional arrows modify the mutation of twin quivers, in particular giving rise to quiver tails. We observed that quiver tails can describe certain sub-configurations of the brane webs obtained via Hanany-Witten transitions, which arise at roots of the Higgs branch in the extended Coulomb branch of the $5d$ theories. We offered evidence of the appearance of tails in various examples and explored the internal consistency of the emerging picture. Below we discuss some directions for future research.

We have seen that, upon mutation, twin quivers with single bidirectional arrows between pairs of nodes naturally give rise to the tail structure associated to the corresponding webs. However, generically, there exist toric phases that result in twin quivers with more than one bidirectional arrow connecting a given pair of nodes. It would be interesting to clarify the web interpretation of the mutations of such quivers and whether they are in correspondence with all the roots of the Higgs branch on the extended Coulomb branch. From this perspective, the tail decoupling of section 5.2 would naturally correspond to entering a Higgs branch of the theory. Note that predicting the number of toric phases for a given toric CY_3 is an open question. Our work suggests an interesting connection between this problem and the classification of roots of the Higgs branch in the extended Coulomb branch of $5d$ theories or, equivalently, of the corresponding brane webs. It would be interesting to explore this correspondence in further detail and determine whether it sheds light on the enumeration of toric phases.

Another question worth investigating is the "surgery" of twin quivers, refining or extending our gluing/removing procedure introduced in sections section 8 and section 5.2 as a method for generating twin quivers for GTPs. Related to this, we have seen that tail decoupling can be used to derive the twin quiver associated to a GTP with white dots. It is thus very natural to ask whether there is an interpretation of this procedure at the level of the original brane tiling. Likewise, one could start with a web with no white dot in the GTP and, upon mutation, find a web described by a GTP with white dots[27] which would naturally lead to the same question. This could provide a hint towards the more ambitious goal of finding

[27]Take for instance the $+_{N,1}$ theory of section 4: for $N > 2$, the analog of our -1 mutation would produce a web encoded in a GTP with white dots.

JHEP10(2024)118

a generalization of brane tilings applicable to generic GTPs. It is expected that such a generalization would encode the BPS quivers of the corresponding $5d$ theories.

Finally, it would be interesting to carry out a detailed study of the moduli spaces of the twin theories and how they depend on the presence of bidirectional arrows, even in the simple case of GTPs without white dots. It is tempting to speculate that bidirectional arrows introduce extra branches in the moduli space of the twin theory related to the tails that appears upon mutation. Moreover, their excision as in section 5.2, could be mapped to entering a Higgs branch and give rise to the twin moduli space for GTPs with white dots. In this respect, it would be very interesting to make contact with the description of the geometries associated to GTPs with white dots presented in [34]. We plan to come back to these issues in the future.

Finally, it would be very interesting to study in more generality to what extent the full extended Coulomb branch is chartered (or, else, what characterizes the special loci which the different phases capture). In section 7 we have concentrated on the family of geometries conifold/$\mathbb{Z}_N$, finding hints of a surprising landscape as N increases. In retrospective, the recent progress in [50] suggests that this precise family might actually be non-generic, as they correspond to free hypermultiplets and consequently, the corresponding GTP's do not have internal points. More generically, it would be very interesting to understand in a unified way the role of the twin quivers and the mutations as described in [50]. Studies along these lines are currently ongoing.

Acknowledgments

We would like to thank Guillermo Arias-Tamargo, Francesco Benini, Sergio Benvenuti, Antoine Bourget, Julius Grimminger and Amihay Hanany for discussions. S.F. would like to thank Rak-Kyeong Seong for previous collaboration on related topics. We would like to acknowledge the Simons Physics Summer Workshop and the Simons Center for Geometry and Physics for hospitality during part of this work. S.F. is supported by the U.S. National Science Foundation grants PHY-2112729 and DMS-1854179. D.R.G. is supported by Spanish national grant MCIU-22-PID2021-123021NB-I00 as well as the Principado de Asturias grant SV-PA-21-AYUD/2021/52177.

Open Access. This article is distributed under the terms of the Creative Commons Attribution License (CC-BY4.0), which permits any use, distribution and reproduction in any medium, provided the original author(s) and source are credited.

References

[1] D.R. Morrison and N. Seiberg, *Extremal transitions and five-dimensional supersymmetric field theories*, *Nucl. Phys. B* **483** (1997) 229 [hep-th/9609070] [INSPIRE].

[2] K.A. Intriligator, D.R. Morrison and N. Seiberg, *Five-dimensional supersymmetric gauge theories and degenerations of Calabi-Yau spaces*, *Nucl. Phys. B* **497** (1997) 56 [hep-th/9702198] [INSPIRE].

[3] M. Del Zotto, J.J. Heckman and D.R. Morrison, *6D SCFTs and Phases of 5D Theories*, *JHEP* **09** (2017) 147 [arXiv:1703.02981] [INSPIRE].

JHEP10(2024)118

[4] D. Xie and S.-T. Yau, *Three dimensional canonical singularity and five dimensional $\mathcal{N} = 1$ SCFT*, *JHEP* **06** (2017) 134 [arXiv:1704.00799] [INSPIRE].

[5] P. Jefferson, H.-C. Kim, C. Vafa and G. Zafrir, *Towards classification of 5d SCFTs: Single gauge node*, *SciPost Phys.* **14** (2023) 122 [arXiv:1705.05836] [INSPIRE].

[6] P. Jefferson, S. Katz, H.-C. Kim and C. Vafa, *On Geometric Classification of 5d SCFTs*, *JHEP* **04** (2018) 103 [arXiv:1801.04036] [INSPIRE].

[7] L. Bhardwaj and P. Jefferson, *Classifying 5d SCFTs via 6d SCFTs: Rank one*, *JHEP* **07** (2019) 178 [*Addendum ibid.* **01** (2020) 153] [arXiv:1809.01650] [INSPIRE].

[8] L. Bhardwaj and P. Jefferson, *Classifying 5d SCFTs via 6d SCFTs: Arbitrary rank*, *JHEP* **10** (2019) 282 [arXiv:1811.10616] [INSPIRE].

[9] F. Apruzzi, L. Lin and C. Mayrhofer, *Phases of 5d SCFTs from M-/F-theory on Non-Flat Fibrations*, *JHEP* **05** (2019) 187 [arXiv:1811.12400] [INSPIRE].

[10] C. Closset, M. Del Zotto and V. Saxena, *Five-dimensional SCFTs and gauge theory phases: an M-theory/type IIA perspective*, *SciPost Phys.* **6** (2019) 052 [arXiv:1812.10451] [INSPIRE].

[11] L. Bhardwaj, *On the classification of 5d SCFTs*, *JHEP* **09** (2020) 007 [arXiv:1909.09635] [INSPIRE].

[12] F. Apruzzi et al., *5d Superconformal Field Theories and Graphs*, *Phys. Lett. B* **800** (2020) 135077 [arXiv:1906.11820] [INSPIRE].

[13] F. Apruzzi et al., *Fibers add Flavor, Part I: Classification of 5d SCFTs, Flavor Symmetries and BPS States*, *JHEP* **11** (2019) 068 [arXiv:1907.05404] [INSPIRE].

[14] F. Apruzzi et al., *Fibers add Flavor, Part II: 5d SCFTs, Gauge Theories, and Dualities*, *JHEP* **03** (2020) 052 [arXiv:1909.09128] [INSPIRE].

[15] L. Bhardwaj, *Do all 5d SCFTs descend from 6d SCFTs?*, *JHEP* **04** (2021) 085 [arXiv:1912.00025] [INSPIRE].

[16] V. Saxena, *Rank-two 5d SCFTs from M-theory at isolated toric singularities: a systematic study*, *JHEP* **04** (2020) 198 [arXiv:1911.09574] [INSPIRE].

[17] F. Apruzzi, S. Schafer-Nameki and Y.-N. Wang, *5d SCFTs from Decoupling and Gluing*, *JHEP* **08** (2020) 153 [arXiv:1912.04264] [INSPIRE].

[18] O. Aharony and A. Hanany, *Branes, superpotentials and superconformal fixed points*, *Nucl. Phys. B* **504** (1997) 239 [hep-th/9704170] [INSPIRE].

[19] O. Aharony, A. Hanany and B. Kol, *Webs of (p,q) five-branes, five-dimensional field theories and grid diagrams*, *JHEP* **01** (1998) 002 [hep-th/9710116] [INSPIRE].

[20] N.C. Leung and C. Vafa, *Branes and toric geometry*, *Adv. Theor. Math. Phys.* **2** (1998) 91 [hep-th/9711013] [INSPIRE].

[21] M. Alim et al., *$\mathcal{N} = 2$ quantum field theories and their BPS quivers*, *Adv. Theor. Math. Phys.* **18** (2014) 27 [arXiv:1112.3984] [INSPIRE].

[22] C. Closset and M. Del Zotto, *On 5D SCFTs and their BPS quivers. Part I: B-branes and brane tilings*, *Adv. Theor. Math. Phys.* **26** (2022) 37 [arXiv:1912.13502] [INSPIRE].

[23] S. Franco et al., *Brane dimers and quiver gauge theories*, *JHEP* **01** (2006) 096 [hep-th/0504110] [INSPIRE].

[24] S. Franco et al., *Gauge theories from toric geometry and brane tilings*, *JHEP* **01** (2006) 128 [hep-th/0505211] [INSPIRE].

JHEP10(2024)118

[25] S. Franco, *Bipartite Field Theories: from D-Brane Probes to Scattering Amplitudes*, *JHEP* **11** (2012) 141 [arXiv:1207.0807] [INSPIRE].

[26] S. Franco, D. Galloni and R.-K. Seong, *New Directions in Bipartite Field Theories*, *JHEP* **06** (2013) 032 [arXiv:1211.5139] [INSPIRE].

[27] S. Franco, *Cluster Transformations from Bipartite Field Theories*, *Phys. Rev. D* **88** (2013) 105010 [arXiv:1301.0316] [INSPIRE].

[28] S. Franco, D. Galloni and A. Mariotti, *Bipartite Field Theories, Cluster Algebras and the Grassmannian*, *J. Phys. A* **47** (2014) 474004 [arXiv:1404.3752] [INSPIRE].

[29] S. Franco, E. García-Valdecasas and A.M. Uranga, *Bipartite field theories and D-brane instantons*, *JHEP* **11** (2018) 098 [arXiv:1805.00011] [INSPIRE].

[30] D. Xie and M. Yamazaki, *Network and Seiberg Duality*, *JHEP* **09** (2012) 036 [arXiv:1207.0811] [INSPIRE].

[31] F. Benini, S. Benvenuti and Y. Tachikawa, *Webs of five-branes and N=2 superconformal field theories*, *JHEP* **09** (2009) 052 [arXiv:0906.0359] [INSPIRE].

[32] M. van Beest, A. Bourget, J. Eckhard and S. Schafer-Nameki, *(Symplectic) Leaves and (5d Higgs) Branches in the Poly(go)nesian Tropical Rain Forest*, *JHEP* **11** (2020) 124 [arXiv:2008.05577] [INSPIRE].

[33] M. Van Beest, A. Bourget, J. Eckhard and S. Schäfer-Nameki, *(5d RG-flow) Trees in the Tropical Rain Forest*, *JHEP* **03** (2021) 241 [arXiv:2011.07033] [INSPIRE].

[34] A. Bourget, A. Collinucci and S. Schafer-Nameki, *Generalized Toric Polygons, T-branes, and 5d SCFTs*, arXiv:2301.05239 [INSPIRE].

[35] S. Franco and R.-K. Seong, *Twin theories, polytope mutations and quivers for GTPs*, *JHEP* **07** (2023) 034 [arXiv:2302.10951] [INSPIRE].

[36] A. Hanany and E. Witten, *Type IIB superstrings, BPS monopoles, and three-dimensional gauge dynamics*, *Nucl. Phys. B* **492** (1997) 152 [hep-th/9611230] [INSPIRE].

[37] O. Bergman and D. Rodríguez-Gómez, *The Cat's Cradle: deforming the higher rank E_1 and $\tilde{E}_1$ theories*, *JHEP* **02** (2021) 122 [arXiv:2011.05125] [INSPIRE].

[38] A. Iqbal, *Selfintersection number of BPS junctions in backgrounds of three-branes and seven-branes*, *JHEP* **10** (1999) 032 [hep-th/9807117] [INSPIRE].

[39] C. Closset, S. Schafer-Nameki and Y.-N. Wang, *Coulomb and Higgs Branches from Canonical Singularities: Part 0*, *JHEP* **02** (2021) 003 [arXiv:2007.15600] [INSPIRE].

[40] B. Feng, A. Hanany, Y.H. He and A. Iqbal, *Quiver theories, soliton spectra and Picard-Lefschetz transformations*, *JHEP* **02** (2003) 056 [hep-th/0206152] [INSPIRE].

[41] S. Franco and G. Musiker, *Higher Cluster Categories and QFT Dualities*, *Phys. Rev. D* **98** (2018) 046021 [arXiv:1711.01270] [INSPIRE].

[42] B. Feng, Y.-H. He, K.D. Kennaway and C. Vafa, *Dimer models from mirror symmetry and quivering amoebae*, *Adv. Theor. Math. Phys.* **12** (2008) 489 [hep-th/0511287] [INSPIRE].

[43] A. Hanany and D. Vegh, *Quivers, tilings, branes and rhombi*, *JHEP* **10** (2007) 029 [hep-th/0511063] [INSPIRE].

[44] O. Bergman, D. Rodríguez-Gómez and C.F. Uhlemann, *Testing AdS_6/CFT_5 in Type IIB with stringy operators*, *JHEP* **08** (2018) 127 [arXiv:1806.07898] [INSPIRE].

[45] A. Hanany and K.D. Kennaway, *Dimer models and toric diagrams*, hep-th/0503149 [INSPIRE].

JHEP10(2024)118

[46] A. Hanany, D. Orlando and S. Reffert, *Sublattice Counting and Orbifolds*, *JHEP* **06** (2010) 051 [arXiv:1002.2981] [INSPIRE].

[47] J. Davey, A. Hanany and R.-K. Seong, *Counting Orbifolds*, *JHEP* **06** (2010) 010 [arXiv:1002.3609] [INSPIRE].

[48] J. Davey, A. Hanany and R.-K. Seong, *An Introduction to Counting Orbifolds*, *Fortsch. Phys.* **59** (2011) 677 [arXiv:1102.0015] [INSPIRE].

[49] K. Hori and C. Vafa, *Mirror symmetry*, hep-th/0002222 [INSPIRE].

[50] G. Arias-Tamargo, S. Franco and D. Rodríguez-Gómez, *The geometry of GTPs and 5d SCFTs*, *JHEP* **07** (2024) 159 [arXiv:2403.09776] [INSPIRE].

[51] S. Franco, S. Lee, R.-K. Seong and C. Vafa, *Brane Brick Models in the Mirror*, *JHEP* **02** (2017) 106 [arXiv:1609.01723] [INSPIRE].

[52] B. Feng, A. Hanany and Y.-H. He, *Phase structure of D-brane gauge theories and toric duality*, *JHEP* **08** (2001) 040 [hep-th/0104259] [INSPIRE].

[53] B. Feng, A. Hanany, Y.-H. He and A.M. Uranga, *Toric duality as Seiberg duality and brane diamonds*, *JHEP* **12** (2001) 035 [hep-th/0109063] [INSPIRE].

[54] B. Feng, S. Franco, A. Hanany and Y.-H. He, *Symmetries of toric duality*, *JHEP* **12** (2002) 076 [hep-th/0205144] [INSPIRE].

[55] A.M. Uranga, *Brane configurations for branes at conifolds*, *JHEP* **01** (1999) 022 [hep-th/9811004] [INSPIRE].

JHEP10(2024)118